



Fisheries New Zealand

Tini a Tangaroa

CCSBT-ERS/2203/12-B
(ERSWG Agenda item 5.1.3)

Hotspot analysis using Antipodean albatross as a test case

Part B: Assessing inter-annual variability in Antipodean albatross distributions in the Southern Hemisphere

Authors: Laura Tremblay-Boyer and Yvan Richard (Dragonfly Data Science)

Prepared for the 14th Meeting of the Ecologically Related Species Working Group (ERSWG14) of the Commission for the Conservation of Southern Bluefin Tuna (CCSBT)

1 Abstract

This study assessed the temporal variability in seabird distributions estimated from tracking data and its impact on a key derived output, the spatial interaction with fishing fleets. Antipodean albatross was used as a case-study given the long-term availability of tracking data for this species and a recent increase in tracking effort across life stages.

The analysis confirmed key spatial differences in the distribution of Antipodean albatross by breeding status, age, and sex. A resampling-based approach was developed to test whether sampling size could lead to biased interpretations of changes in distributions through time. The approach was applied to a well-represented group with high-quality tracking data (GPS-tagging data from non-breeder females), and highlighted that low track sample sizes can influence key features of the estimated species distribution, such as the areal extent. The resampling approach was expanded to test for differences in distribution overlap across time periods via randomisation. This exercise found that other track features, such as the track length (measured in the number of observations), also needed to be accounted for when comparing distributions across time periods. This is especially relevant to seabird species where multiple tag types have been used throughout the tracking time series.

An improved distribution map of all life stages combined was produced, which integrated all available tracking data with weights by life stage from a recently-updated population model. The distribution map was compared with surface-longline fishing effort in the Southern Hemisphere to assess variability in interaction hotspots. Although there was variability in the location of interaction hotspots through time, there were distinct areas that were consistently classified as hotspots over the time period from 1997 to 2021. These areas included the Tasman Sea, an area eastward and northward of New Zealand's North Island, and the Chilean Coast. The approach of assessing hotspot areas and their consistency through time with the overlap statistic used here is broadly applicable to other seabird species with tracking data.

2 Introduction

Species distributions for seabirds can be difficult to quantify because individuals have an extensive range but use specific areas intensively. In addition, area use can change over time and across breeding status. A previous assessment of the risk of surface-longline fisheries for albatrosses and petrels in the Southern Hemisphere was presented to CCSBT in 2019 (Abraham et al. 2019). This assessment developed distributions for key life stages of 26 seabird taxa (including two sub-species for Antipodean albatross, *Diomedea antipodensis antipodensis* and *D. a. gibsoni*) from tracking data, following a methodology similar to that described by Carneiro et al. (2020). Seabird distributions are particularly important in the application of spatial risk assessment approaches to inform management, because seabird distributions and fishing effort data are combined to generate predictions of particular areas of high capture. This identification of "hotspots" has been proposed as a tool for the spatial

management of the surface-longline fishery in the Commission for the Conservation of Southern Bluefin Tuna (CCSBT) convention area.

The previous analysis by Abraham et al. (2019) highlighted three limitations for the development of seabird distributions from tracking data: first, tracking data were not available for all species, life stages, and sites, so that distribution data needed to be augmented with existing range maps that lacked density information; second, the generated distributions were static, i.e., all available tracking data were combined into a single distribution applied to all years; if seabird distributions vary between years, any management relying on the average location of hotspots across years might not be effective; third, distributions derived from observations only are dependent on the behaviour of individual birds, and high-use areas might be excluded by chance if none of the tracked individuals use them during tracking. This latter aspect is especially of concern for species for which little tracking data are available.

A key challenge for attempting to address these limitations was the availability of tracking data for most seabird species. Nevertheless, since then, there have been 158 000 new locations recorded for the Antipodean albatross sub-species *D. a. antipodensis*. In addition, previous research has already identified potential changes in the distribution of this species for some life stages (Carneiro et al. 2020). Based on this data-rich tracking dataset, the Antipodean albatross was used here as a case study to explore some of the limitations raised in the previous analysis by Abraham et al. (2019). In the present study, the temporal variability in distributions was re-assessed in view of the availability of tracking data throughout the time series. This re-assessment included the development of an approach to test for changes in distribution between time periods. It also included the application of a hotspot metric across life stages and over time to assess variability in high-use areas. In addition, a life-stage weighted distribution for all individuals was generated and compared with surface-longline effort data from the Southern Hemisphere.

3 Methods

3.1 INPUT TRACKING DATA AND DATA PREPARATION

All available tracking data for Antipodean albatross from 1997 onwards were acquired from the New Zealand Department of Conservation, with permission from private data holders when applicable. We note that the 2019 risk assessment used an externally prepared version of this dataset (from the Birdlife International Seabird Tracking Database); however, as recent tagging years for Antipodean albatross were missing from this dataset, the data preparation was carried out again for internal consistency, based on the original tracking data for the period from 1997 to 2021.

Tracking data were collected using tracks from PTT (platform transmitting terminal), GLS (global location sensor), and GPS (global positioning system) tracking devices for the period from 1997 to 2021. Geographical coordinates were directly available for PTT and GPS tags (either from the device itself for GPS tags or via the device provider for PTT tags). For GLS tags, locations were estimated from the sunlight measurements and sea surface temperature

recorded by the tracking device. The probGLS algorithm (Merkel et al. 2016) was used to generate a most-likely track from the median of the predicted locations for each observation. This approach estimates location with an error of less than 200 km (Merkel et al. 2016), but precision changes throughout the year, and is lower close to the equinoxes. Once a most-likely track was estimated for GLS tags, all locations for PTT, GLS, and GPS tags were collated into a single dataset.

Life-history covariates were also available from the data provider, including the breeding status at the moment of tagging, sex, and age of tagged individuals. For analyses comparing adult distributions according to breeding status, individuals were classified as breeders if their status was “Breeder” or “Nester”; they were classified as non-breeders if their status was “Failed breeder”, “Failed nester”, “Non-breeder”, “Pre-breeder” or “Bird On Ground (BOG)”. In addition, a more refined breeding status (i.e., for the full time period, not just at tag release) was available for some individuals from a recent demographic study (Richard 2021). This information is particularly valuable for interpreting the tracks classified under “Breeder” at tag release, because unsuccessful breeding can lead to changes in distribution. This breeding status was used when available, otherwise the breeding status at release was assumed to be the same for the entire time period spanned by a track. Age was also available from the demographic study for some individuals. All individuals of age 7 or less were classified as juvenile; if age was unavailable, the initial classification at tag release was used.

Records of individual bird locations were prepared using the following set of rules:

- records were removed if locations or dates were outside of latitudes 90°W to 90°E and time period 1997 to 2021;
- records were removed if the speed of an individual from a previous location or to the next location (in km/h, based on great circle distances) was in excess of 100 km/h;
- gaps in the tracking data of longer than 24 hours were discarded by splitting the deployment into separate segments;
- the first and/or last segments were removed if they contained less than 10 observations and were more than three months from the second and second-to-last segments, respectively;
- single segments were removed when they contained a single observation that was more than 1000 km from previous or next segments;
- the start and/or end record within each segment was removed if the longitude or latitude were outside of the 0.5th to 99.5th quantile range for these values for the individual bird track, and if the speed to and from the record was in excess of 100 km/h.

The error in positions estimated for GLS tracks increased close to the equinoxes. This increase can result in strong latitudinal patterns that may not be representative of true bird position. For this reason, estimated GLS latitudes outside of the range measured from PTT and GPS tracks were removed from the dataset.

There were 345 individual tracks following the data preparation.

The prepared location records were interpolated at regular time intervals of 30 minutes within each segment, assuming linear displacement between records. No locations were interpolated between separate segments. The interpolated records were assumed to reflect occupancy over the spatial range of the study. The first three days following deployment were removed from the dataset to reduce a spatial bias caused by seabirds being tagged at the colony.

Following Abraham et al. (2019) and Carneiro et al. (2020), the gridded distributions were then generated by summing over all the interpolated records in each pixel of a pre-defined distribution grid. If needed, the density can be standardised so that all cells weighted by their area summed to 1. Distribution grids were defined at both the 1-degree resolution or at the 5-degree resolution. The latter resolution matches the resolution of surface-longline effort datasets and corresponds with the spatial resolution used in risk assessments. When applicable, records were first divided into categories (sex, breeding stage, year) before aggregation.

3.2 ESTIMATING THE PROBABILITY OF CELL INCLUSION IN THE DISTRIBUTION

A resampling approach was trialled to estimate the influence of the availability of tracking data on the size of the generated seabird distribution. The approach was implemented on data for female non-breeders, using only GPS tracks for consistency ($n = 25$).

Individual tracks were randomly selected n times (without replacement) from the sample dataset, and a distribution was generated from this sub-sample. For this preliminary test, the resampling was repeated 100 times for track sample size (' n ') from 3 to 22. For each track sample size scenario ' n ' the probability of cell inclusion in the final range was calculated from the proportion of times the cell was present in the distribution generated from each of 100 sub-samples. The high-probability area (in number of cells) of the final range was calculated by summing the number of cells with a probability of inclusion greater than 0.95. The resampled areas were compared with the area of the distribution obtained when all 25 tracks were included in the estimated distribution.

3.3 COMPARING DISTRIBUTIONS BETWEEN TIME PERIODS

An approach was developed to test for differences between the distribution of individuals across different time periods. The approach was tested on male and female non-breeders for the time periods pre-2004 and post-2011. This period was chosen because differences in distributions between the time periods pre-2004 and 2011–2017 were previously noted for these two groups (Elliott & Walker 2017). The periods also capture changes in tagging methods, particularly in the type of tag used (PTT-only pre-2004, and a mix of PTT, GLS and GPS thereafter) and overall tagging numbers. As such, the approach also allows testing of whether changes in tagging methodology can influence the distribution generated from tagging data.

The approach used both resampling and randomisation to test for differences in time periods while accounting for differences in sample size across time periods and differences in track lengths. The reference period included years 1997 to 2004 (pre-2004) and the test period was

defined to be the years from 2011 to 2021 (noting no new tags were released from 2005 to 2010). The prepared tracking dataset was filtered to include only non-breeding adults, based on the integrated population model (IPM) definition when available, or the status at release when the IPM definition was lacking. The dataset was then split by sex and time period, and a test of differences in distribution was run separately for males and females.

For each sex, a kernel density was estimated from tracks selected from the reference and test time periods, using the kernelUD function from the adehabitatHR package (Calenge 2006). All tracks were selected from the reference dataset, given the limited sample size, and a matching number of tracks was randomly selected from the test dataset. There were five tracks available for the pre-2004 period for non-breeding females, and 10 tracks available for the pre-2004 period for non-breeding males. The overlap between the 95% kernel outlines for the two periods was then measured using the Bhattacharyya's affinity (BA), a metric of spatial overlap between distributions which ranges from 0 (no overlap) to 1 (full overlap) (Fieberg & Kochanny 2005). This measurement was repeated 500 times.

To provide a probabilistic framework to test for a difference in distributions between time periods, the above procedure was repeated with time periods that were randomly assigned to individual birds before the kernel density was built (retaining the same number of tracks for each time period). The values of the resulting BA were then compared, pair-wise, with the corresponding values from the non-randomised BA to compute the proportion of times the non-randomised BA was smaller than the randomised BA. If there was no difference in distributions through time, the distributions of BA for the non-randomised and the randomised versions of the test are expected to be similar. If there is a difference in distributions through times (indicated by smaller values of BA, as the metric approaches 0 as overlap decreases), the non-randomised BA is expected to be smaller than the randomised version.

A modification to the above procedure was applied separately to test for the influence of changing track lengths through time. Here, the resampled test dataset was further modified to match the track lengths in the reference datasets. Track lengths (in number of records) for the reference birds were randomly re-assigned to the individual birds in the test dataset. Track length for these birds was then shortened to match the reassigned track length, starting from the first record. When the re-assigned track length was longer than the number of records available for a test bird, all records for this test bird were retained. The testing procedure was otherwise repeated to generate non-randomised and randomised distributions of the BA metric.

3.4 IDENTIFYING DISTRIBUTION HOTSPOTS

Distribution hotspots were quantified for the entire tracking dataset and for subsets by breeding status and/or year. The Getis-Ord G_i^* statistic was used as it both detects hotspots and provides a statistical framework to test for their significance (Getis & Ord 1992, see also Sussman et al. 2019 for a review of hotspot metrics). The G_i^* statistic searches for spatial clusters of data points for each grid cell in comparison to its neighbours. The resulting z-score can be assessed for significance, with higher values more likely to be statistically significant.

Neighbour cells were defined as cells that share a border with the focal cell (i.e., each cell has four neighbours, except for cells at the edge of the grid), using the function *poly2nb* in the R package *spdep*. The G_i^* statistic was computed using the function *localG* (also from the R package *spdep*).

The G_i^* value was calculated for each cell and year, and hotspots were identified by selecting the cells with a z-score above 2.575829, corresponding to a confidence level of 99%. The inter-annual stability of hotspots was calculated as the proportion of years when the cell was selected as a hotspot.

3.5 INTERACTIONS BETWEEN ANTIPODEAN ALBATROSS AND SURFACE-LONGLINE FISHERIES

To assess variability in interaction hotspots between Antipodean albatross and surface-longline fishing effort, a single, all stage-combined distribution was first derived at the 1-degree scale. This distribution combined the tracking data from all years, and could not be produced for separate years due to the lack of tracking of most demographic strata.

For the stage-combined distribution, a single at-sea distribution of Antipodean albatross was derived by combining the distribution of each demographic stratum — a combination of age class (juvenile, pre-breeder, adult), breeding status and success (adult non-breeder, successful breeder, or unsuccessful breeder), and sex (male or female).

For the distribution of each stratum, the count of tracking locations in each 1-degree by 1-degree grid cell was used as a proxy of bird density. The density was then normalised, taking into account the area of each cell, to obtain a density in square km. It was then smoothed for cells with less than five birds or on the edge by taking a weighted average of the eight neighbouring cells, using weights of 1.0, 0.5, and 0.25, for the focal cell, the cells immediately adjacent, and the diagonal cells, respectively. Finally, the density was multiplied by the number of birds in the stratum, obtained from a Bayesian integrated population model of the species (Table 1; Richard 2021).

The population model was fitted to capture-recapture data collected every year since 1994 within a subset of the whole colony at Antipodes Island. The population structure was simulated over the study period, modelling the fate of each individual using the state transitions estimated in the model; the structure of the simulated population in 2021 was used to provide the number of individuals in each stratum. The studied population was then scaled up to the entire population based on the studied population representing 2.7332% of the total population, following population surveys of the entire island between 1994 and 1996.

The density of each stratum was summed across all strata to derive the final at-sea distribution, with a density expressed in birds.km⁻².

A dataset of surface long-line fishing effort was collated by the National Institute of Water and Atmospheric Research (NIWA) from data provided by Regional Fisheries Management

Organisations (RFMOs), gridded at a resolution of 5 degrees by 5 degrees. This dataset is meant to include all surface-longline fishing effort in the Southern Hemisphere. The data were provided for the period 1952 to 2019, but were filtered to only include years since 1997, corresponding with the period for which tracking data were available.

The grid of fishing effort was first converted to a resolution of 1-degree by 1-degree to match the resolution of the bird distribution, after multiplying the effort from each 5-degree cell by the area of the cell relative to that of the covering 5-degree cell to obtain the effort for each 1-degree by 1-degree cell (i.e., assuming that effort was distributed evenly across each 5-degree cell). The resolution was increased to 1 degree to retain a maximum amount of information from the Antipodean albatross distribution.

Overlap between surface-longline fisheries and Antipodean albatross was calculated by multiplying the fishing effort (in hooks) and the bird density (in birds.km⁻²) in each grid cell.

The overlap was calculated for each year of fishing, and the hotspot statistic G_i^* was calculated (as described in section 3.4). Hotspot consistency amongst year was assessed by counting the number of times each cell was assigned to a hotspot with 99% confidence.

4 Results

4.1 CHARACTERISTICS OF THE INPUT DATASET

Following the data preparation, tracking data were available for Antipodean albatross for tags deployed between 1997 and 2001, 2003 and 2004, and 2011 to 2021 (Figure 1). The number of tags with data available each year was below 20 for all years up to 2019; subsequently, the number of tags increased to over 60 tags each in 2019 and 2020. For the last year of the study (2021), data were only available from about 40 tags, because some devices have yet to be recovered.

There were some changes in the tagging devices deployed over time: PTT devices were deployed exclusively up to 2004, then GLS devices between 2011 and 2018; GPS devices were first deployed in 2019, together with additional PTT and GLS devices (Figure 1).

Tag data for both males and females were available for each year of the time series, with a slightly higher proportion of females but no pronounced trend in the repartition (Figure 1). Tags were deployed almost exclusively on adults up to 2019, after which more than a third of deployed tags were on juveniles (except in 2021, but noting some tags are yet to be recovered).

The distribution of breeding status has changed over time, with a higher proportion of breeders in earlier tagging years (Figure 1).

Track length, measured in days with at least one recorded position, varied over time; most tag data from the earlier time period were shorter than six months (Figure 2). For data from tags between 2011 and 2018, when all tags were of type GLS, the tracks often exceeded one year in length (with some tracks spanning up to two years).

4.2 TRENDS IN DISTRIBUTIONS BY LIFE STAGE AND OVER TIME

There were some differences in the estimated unstandardised distributions of Antipodean albatross, depending on the life stage and over time (Figures 3 to 9). The overall distribution showed areas of high use around the main colony of Antipodes Island and in surrounding waters, and in two distinct areas along the west coast of South America (Figure 3). There was also relatively high use of Tasman Sea by individuals, but to a lesser extent. Considering the overall distribution at a lower resolution (from a 1- to 5-degree grid) showed the same trends with less precise delineation of high-density hotspots (e.g., along the west coast of South America)(Figure 4).

State-specific trends in spatial use emerged when the distributions were disaggregated by age and breeding status (Figures 5 to 9). Juveniles used waters eastward of North Island New Zealand and the Tasman Sea extensively, but travelled smaller distances than adults (Figure 4). Female breeders had a restricted distribution centred on Antipodes Island, but non-breeders foraged across the Pacific Ocean, including in areas on the west coast of South America (Figures 6 and 7). Similarly, male breeders also foraged closer to Antipodes Island, whereas the distribution of male non-breeders extended eastward including the west coast of South America (Figures 8 and 9). Male non-breeders appeared to use a wider latitudinal range than any of the other groups (Figure 9).

Distribution time series (grouped by observation year; Figures 10 to 13) captured the key spatial trends evident in the aggregated map versions, but with particularly high inter-annual variability in years with low sample sizes.

4.3 INFLUENCE OF TRACKING DATA AVAILABILITY ON DISTRIBUTION SIZE

A resampling approach was developed to quantify the influence of sample size on estimated distributions. It was then tested on a subset of the tracking data with high position accuracy (GPS tracks from female non-breeders). There were 25 tracks available for this subset, spanning 2019 and 2020, with observed positions ranging from the Tasman Sea to the eastern Pacific Ocean (Figure 14).

Distributions were generated from 100 random subsets of these tracks (see Figure 15 as an example). As the number of tracks sampled increased from 3 to 10, the core range (defined

here as the area where cells were included in more than 95% of the samples) expanded from the area eastward of Antipodes Island to the west coast of South America (Figure 16). When 20 tracks (i.e., 80% of the full dataset) were included in the sample, additional cells in upper or lower latitudes were included with higher probability. The longitudinal range was mapped with higher probability at lower sample sizes than the latitudinal range, indicating that fewer individuals used higher or lower latitudinal bands compared with the core longitudinal area; this finding indicated that a higher sample size might be required to characterise the full extent of the latitudinal range.

The area of the core range showed the highest increase from subsamples of 3 to 10 tracks, with a slower rate thereafter (Figure 17).

4.4 POST-2011 CHANGES IN THE DISTRIBUTION OF NON-BREEDERS

A hybrid resampling-randomisation approach was developed to test for changes in distribution between two time periods while accounting for sample size and track length changes. The approach was applied to female and male non-breeders in separate analyses (Figures 18 and 19). When track length was not standardised between time periods, there was evidence ($Pr = 0.83$) that there was a change in distribution between the pre-2004 and the post-2011 period (Figure 18, top right). However, once track length was standardised across time periods there was no difference in the overlap metric measured between observed and randomised samples ($Pr = 0.51$; Figure 18, bottom right).

In general, the overlap between pre-2004 and post-2011 distributions was higher for non-breeding males than for non-breeding females (approximately 0.75; Figure 19, right column). There was evidence of a difference between pre-2004 and post-2011 time periods ($Pr = 0.84$), but the predicted difference was lower. Accounting for track length across time periods slightly reduced the probability of difference between time periods ($Pr = 0.77$).

4.5 DISTRIBUTION HOTSPOTS AND HOTSPOT VARIABILITY THROUGH TIME

There were clear differences in the distribution of density hotspots between life stages (Figure 20). All life stages used the area immediately east of New Zealand intensively, with the highest use adjacent to the colony (Antipodes Island). Nevertheless, juveniles also heavily used some areas in the Tasman Sea, especially westward from the New Zealand Exclusive Economic Zone. Non-breeding adults had hotspots distributed across the South Pacific Ocean, including in the Tasman Sea, an area extending eastward of New Zealand along the 40°S parallel, and an extensive area off the Chilean coast at around latitude 44 degrees South and around the Juan Fernández Islands. Breeders had the most restricted hotspot area, concentrated around Antipodes Island, and extending northward to the tip of New Zealand.

When considering density hotspots for all life stages through time, there was some variability evident; earlier years with few tagged individuals showed the most variability compared with later years, when more data were available (Figure 21). There was some variability between years regarding a hotspot in the Tasman Sea, and also in the spatial extent of the hotspot area off the coast of Chile. When cells were classified as a function of the proportion of times they were classified as a hotspot with a 99% confidence level, the two areas with the highest hotspot consistency were the areas eastward of New Zealand, including Antipodes Island and the Chilean coast (Figure 22).

4.6 VARIABILITY IN THE INTERACTION WITH THE SURFACE-LONGLINE FLEET

The combined at-sea distribution for all life stages of Antipodean albatross reflected the extensive range of this species in the Southern Hemisphere, from the west coast of Australia in the Indian Ocean to the Chilean coast in the east Pacific Ocean (Figure 23). The north end of the distribution was approximately bounded by the 25°S parallel. Surface-longline fishing effort for years 1997 to 2019 was higher on the western side of the South Pacific Ocean and also north of the 20°S parallel, but effort was distributed throughout the South Pacific Ocean (Figure 24). Overall overlap varied between years and amongst fleets, with a peak in 2003 and a plateau from 2007 onwards (Figure 25). The two fleets with the highest overlap were the New Zealand and the Japanese surface longline fleets. The areas with the highest consistency in interaction hotspots throughout the time period were the Tasman Sea (skewed towards the Australian east coast), an area including waters east and north of New Zealand's North Island, and the Chilean coast (Figure 26). The spatial overlap between surface-longline fisheries and Antipodean albatross for years 1997 to 2019 is included in Figure 27.

5 Discussion

This analysis highlighted key spatial differences in the distribution of Antipodean albatross by breeding status, age, and sex; it also further delineated the distribution of juvenile birds given increased tagging for this group in the 2020 and 2021 breeding seasons. An improved distribution map was produced with all life stages combined, integrating all available tracking data with weights by life stage from a recently-updated population model. The distribution map was compared with surface-longline fishing effort in the Southern Hemisphere to assess variability in interaction hotspots. Although there was variability in the location of interaction hotspots through time, there were distinct areas that were consistently classified as hotspots over the time period from 1997 to 2021. These areas included the Tasman Sea, an area eastward and northward of New Zealand's North Island, and the Chilean Coast.

Spatial overlap between Antipodean albatross and the surface longline fleet was found to be highest for the New Zealand and Japanese fleets. This differs from the results of Bose & Debski (2020) who found highest overlap for the fleets of the Fishing Entity of Taiwan and Vanuatu, and minimal overlap with the Japanese fleet for the year 2019. However, there were some key differences in methodology, most notably their effort dataset was collated from the Global Fishing Watch and their effort variable was measured in hours. For the year 2019 only, the current analysis found the Fishing Entity of Taiwan's fleet to have the highest overlap followed by the Japanese fleet, which confirms the importance of the Fishing Entity of Taiwan's fleet when quantifying interactions. However, any estimates of overlap (and resulting captures) could vary depending on the effort dataset used to inform the analyses.

A key challenge when developing seabird distributions from tagging data is that sampling sizes are often uneven across time and breeding stages, leading to uncertainty about the reliability of the estimated distributions and derived products such as interaction hotspots with fisheries. A resampling approach was developed here to test whether sampling size could lead to biased interpretations of changes in distribution through time. The approach was applied to GPS-tagging data from non-breeder females, and confirmed that low track sample sizes can influence key features of the estimated species distribution, such as the areal extent. For this reason, different time periods with different tag availability should not be compared directly without accounting for this factor, as the extent of the distribution tends to expand with sample size (especially at low sample sizes).

Variability in track duration (the number of records available for each track) can also impact the interpretation of distributional shifts. This aspect is especially relevant for Antipodean albatross for which the tagging dataset extends to more than 20 years with many changes in tagging methodology throughout. For example, GLS tags tended to remain active for a considerably longer period of time than PTT tags, which impacted the comparison of distributions for non-breeders between periods if PTT tags were used exclusively in some years. We were unable to confirm a previously reported eastward shift in the distribution of non-breeding females post-2011 once track duration was accounted for. Nevertheless, the sample size for this group pre-2004 was small, so statistical power to detect a difference would be low.

The characterisation of density hotspots for key life stages highlighted two high-use zones beyond the area expected around the breeding colony: the Tasman Sea was especially important to juveniles (and to non-breeding adults, to a lesser degree), whereas the Chilean east coast was especially important to non-breeding adults. These spatial patterns were not apparent for all years, which could reflect the different availability of tracks by life stages through time, and other factors such as long-term oceanography cycles like El Niño. When considered across the time-series, however, these areas were consistently shown as hotspots, increasing confidence in the reliability of their classification. The approach of assessing hotspot areas and their consistency through time using the G_i^* statistic is broadly applicable to other seabird species with tracking data.

The hotspot consistency approach was expanded to also assess interaction hotspots between Antipodean albatross and surface-longline fisheries; it succeeded in identifying areas with high interactions through time. One challenge in this application was the low resolution of the surface-longline effort dataset, which obscured some spatial patterns in the species'

distribution. By increasing the resolution of the effort dataset, a higher-resolution delineation of interaction hotspots was obtained, but this approach relied on the assumption that effort was evenly distributed across 5-degree cells. Effort data recorded at a higher resolution would improve precision in the identification of interaction hotspots. Also, the temporal variability in overlap was driven entirely by changes in fishing effort, as a stationary distribution of Antipodean albatross was used due to the uneven coverage of the tracking dataset across demographic strata for most years. Additional data on fishing effort for 2020 and 2021 combined with the existing 2019 fishing effort data could inform a comparison with annual bird distributions for the period 2019 to 2021 (which has better coverage across demographic strata).

One practical consideration when assessing changes in spatial distribution by life stage is that the breeding status is often only available at the time of tag release. However, if a breeding individual is unsuccessful, its foraging distribution is likely to expand; not accounting for this change in breeding status might lead to errors in the estimated distribution, particularly for breeding individuals. Here we were able to access a separate dataset with detailed breeding status information by individuals from a population model (see Richard 2021). When only tracking data are available, another approach could be to reclassify breeders as non-breeders if they have been absent from the colony beyond a threshold period of time (e.g., applied in Bose & Debski 2020). This aspect is also relevant to non-breeding individuals if the tag duration extends into the next breeding season, and needs to be considered when developing life-stage specific distributions for seabirds.

The resampling approach used here was focused on testing hypotheses with practical applications for the interpretation of tracking data; e.g., whether range expansion or distributional shifts could be determined between time periods with different sampling sizes and/or track durations. Other advantages of a resampling approach include the identification of track sample size thresholds below which the generated distributions are unlikely to be representative. Probability distributions for metrics of interest (e.g., the probability of cell inclusion in the distribution) could also be propagated to other components of a risk assessment analysis (e.g., hotspot delineation and capture estimates).

6 Acknowledgments

We would like to thank Samhita Bose at the New Zealand Department of Conservation, and Kath Walker and Graeme Elliott for providing access to the tracking dataset and assisting with the interpretation. The Aquatic Environment Working Group (hosted by Fisheries New Zealand) provided valuable feedback on an earlier version of this analysis. This project was funded under Fisheries New Zealand project PRO2021-06.

7 References

Abraham et al. (2019) - Abraham, E.; Richard, Y.; Walker, N.; Gibson, W.; Daisuke, O.; Tsuji, S.; Kerwarth, S.; Winkler, H.; Parsa, M.; Small, C.; Waugh, S. (2019). Assessment of the risk of surface

longline fisheries in the Southern Hemisphere to albatrosses and petrels, for 2016. Prepared for the 13th meeting of the Ecologically Related Species Working Group (ERSWG13) of the Commission for the Conservation of Southern Bluefin Tuna (CCSBT). Retrieved from https://www.ccsbt.org/en/system/files/ERSWG13_17_NZ_Assessment_RiskOfSurfaceLonglineFisheries_SouthernHemisphere.pdf.

Bose, S. & Debski, I. (2020). Antipodean albatross spatial distribution and fisheries overlap 2019. Department of Conservation Technical Report. 23 p.

Calenge C (2006). The package adehabitat for the R software: tool for the analysis of space and habitat use by animals. *Ecological Modelling*, 197, 1035.

Carneiro, A.P.; Pearmain, E.J.; Opper, S.; Clay, T.A.; Phillips, R.A.; Bonnet-Lebrun, A.-S.; Wanless, R.M.; Abraham, E.; Richard, Y.; Rice, J., et al. (2020). A framework for mapping the distribution of seabirds by integrating tracking, demography and phenology. *Journal of Applied Ecology* 57: 514–525

Elliott, G.; Walker, K. (2017). Antipodean wandering albatross census and population study 2017. Report by Albatross Research. 20 p.

Fieberg, J., & Kochanny, C. O. (2005). Quantifying home-range overlap: The importance of the utilization distribution. *The Journal of Wildlife Management*, 69(4), 1346-1359.

Getis, A., & Ord, J. K. (1992). The analysis of spatial association by use of distance statistics. *Geographical Analysis* 24(3): 189–206.

Merkel, B.; Phillips, R.A.; Deschamps, S.; Yoccoz, N.G. (2016). A probabilistic algorithm to process geolocation data. *Movement Ecology* 4:26.

Richard, Y. 2021. Integrated population model of Antipodean albatross for simulating management scenarios. BCBC2020-09 final report prepared by Dragonfly Data Science for the Conservation Services Programme, Department of Conservation. 31 p. Retrieved from <https://www.doc.govt.nz/globalassets/documents/conservation/marine-and-coastal/marine-conservation-services/reports/final-reports/bcbc2020-09-antipodean-albatross-simulations-final-report2.pdf>.

Sussman, A.L., Gardner, B., Adams, E.M., Salas, L., Kenow, K.P., Luukkonen, D.R., Monfils, M.J., Mueller, W.P., Williams, K.A., Leduc-Lapierre M., Zipkin, E.F. (2019). A comparative analysis of common methods to identify waterbird hotspots. *Methods in Ecology and Evolution* 10(9): 1454–1468.

8 Appendix

8.1 TABLES

Table 1. Number of individuals in each demographic stratum used to weigh the stratum-level at-sea distributions, obtained from an integrated population model of Antipodean albatross (Richard 2021).

Status	Gender	Individuals
Juvenile	Female	2244
	Male	2144
Pre-breeder	Female	2181
	Male	3752
Non-breeding adult	Female	3292
	Male	7162
Unsuccessful breeder	Female	1106
	Male	1282
Successful breeder	Female	2188
	Male	2542

8.2 FIGURES

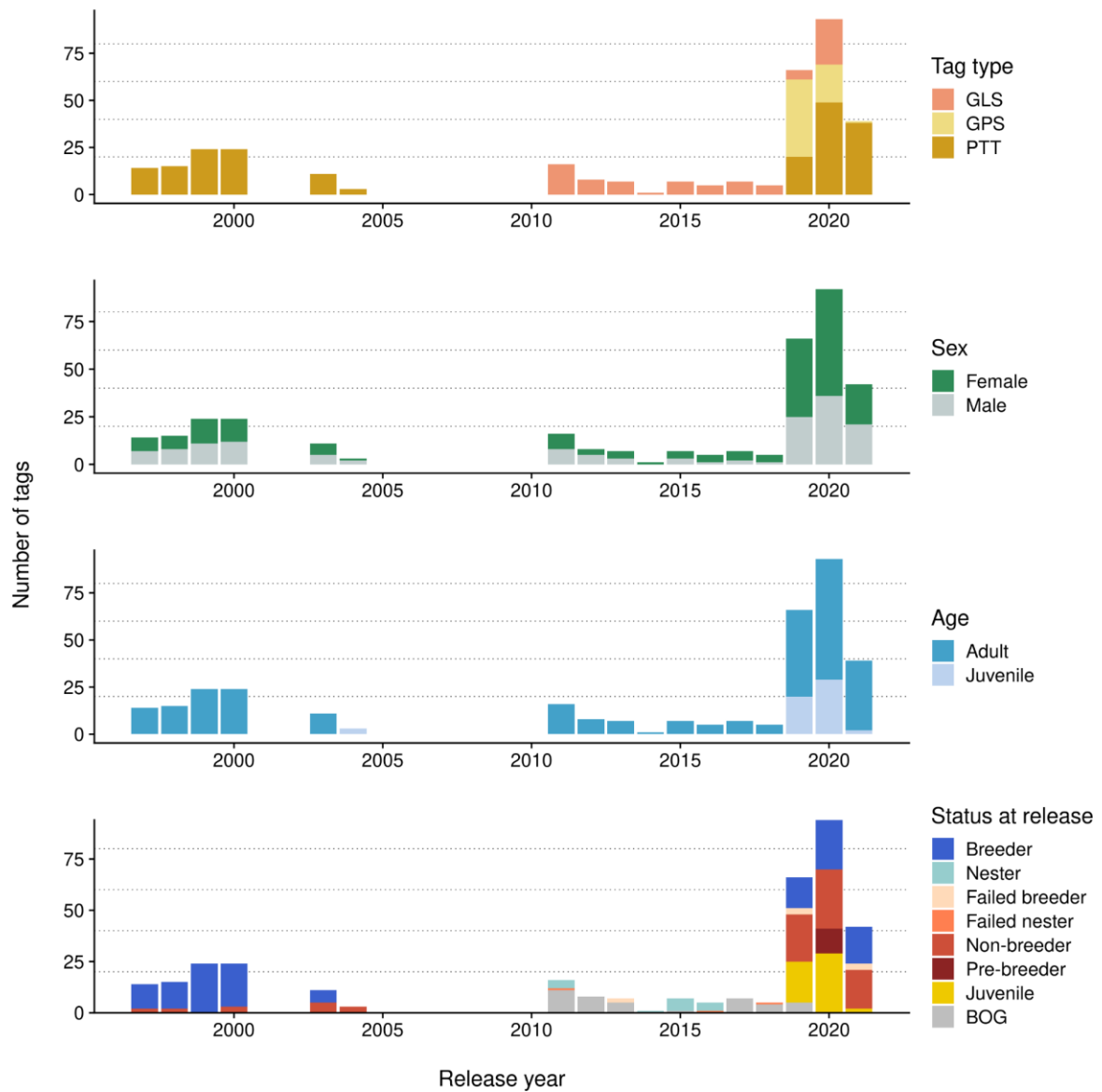


Figure 1. Overview of prepared tracking dataset for Antipodean albatross by type of tagging device, individual sex, age, and breeding status at tagging (BOG=Bird On Ground).

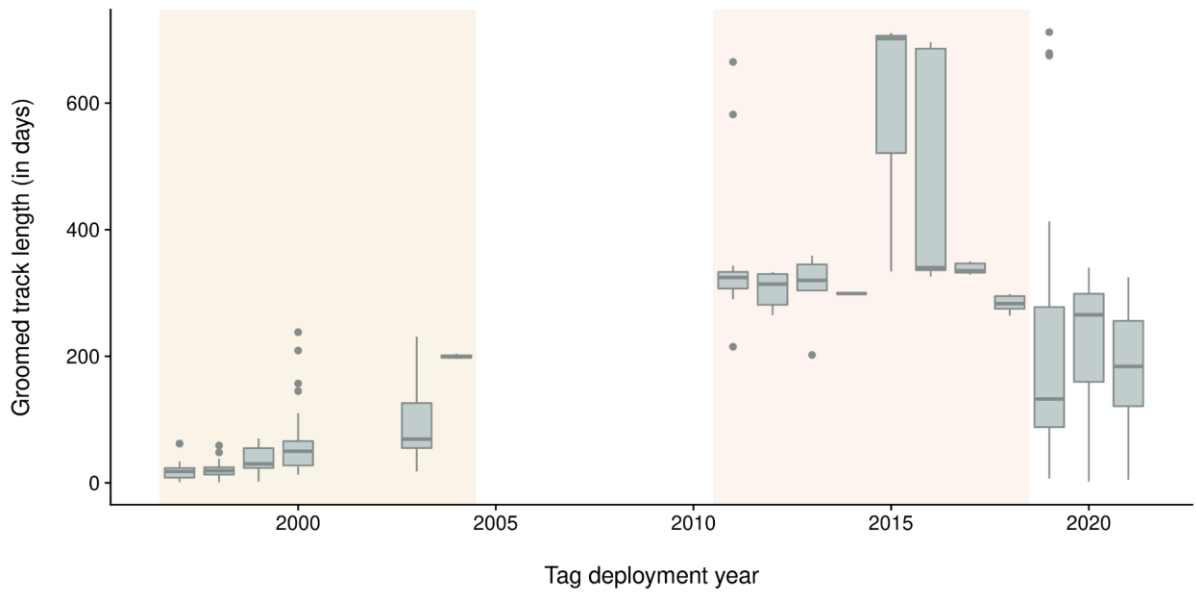


Figure 2. Distribution of track length (in number of days) by individual Antipodean albatross tagged, shown by release year. The boxplot shows the interquartile range, with the median as a bold horizontal line. The light yellow and pink boxes highlight periods when all tags were of type PTT ((platform transmitting terminal) and GLS (global location sensor), respectively.

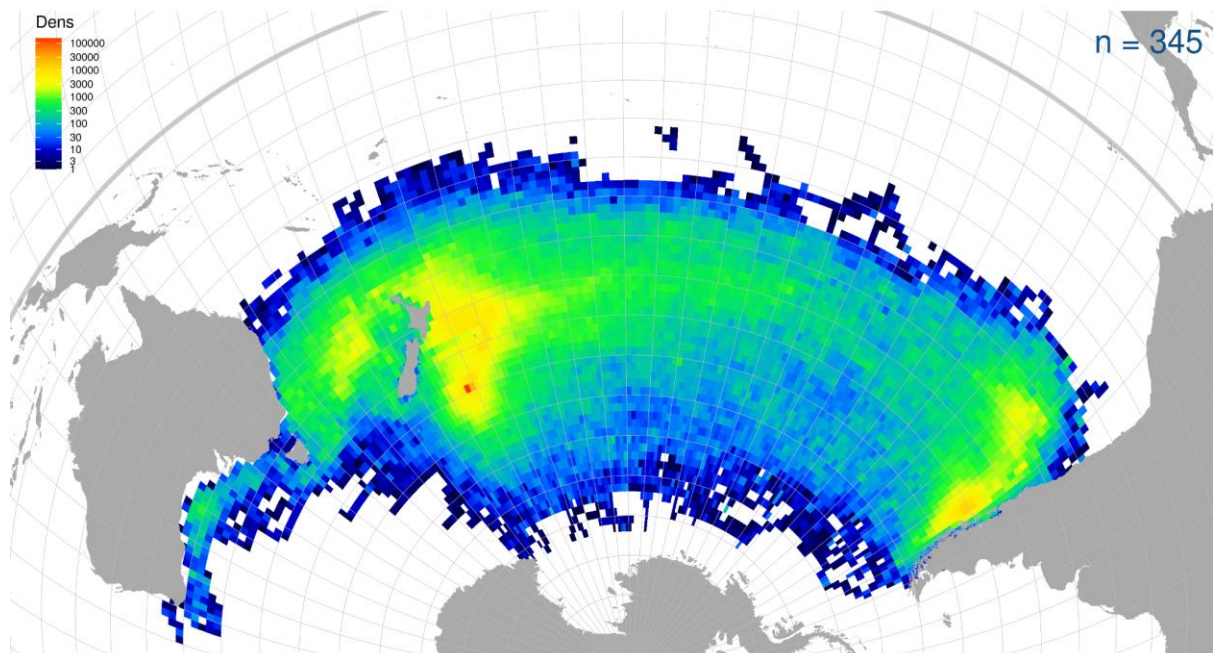


Figure 3. Density (in log-scale) of interpolated tag records for all years and tracked Antipodean albatross individuals combined, at 1-degree resolution. The number of tracks is shown in the top-right corner.

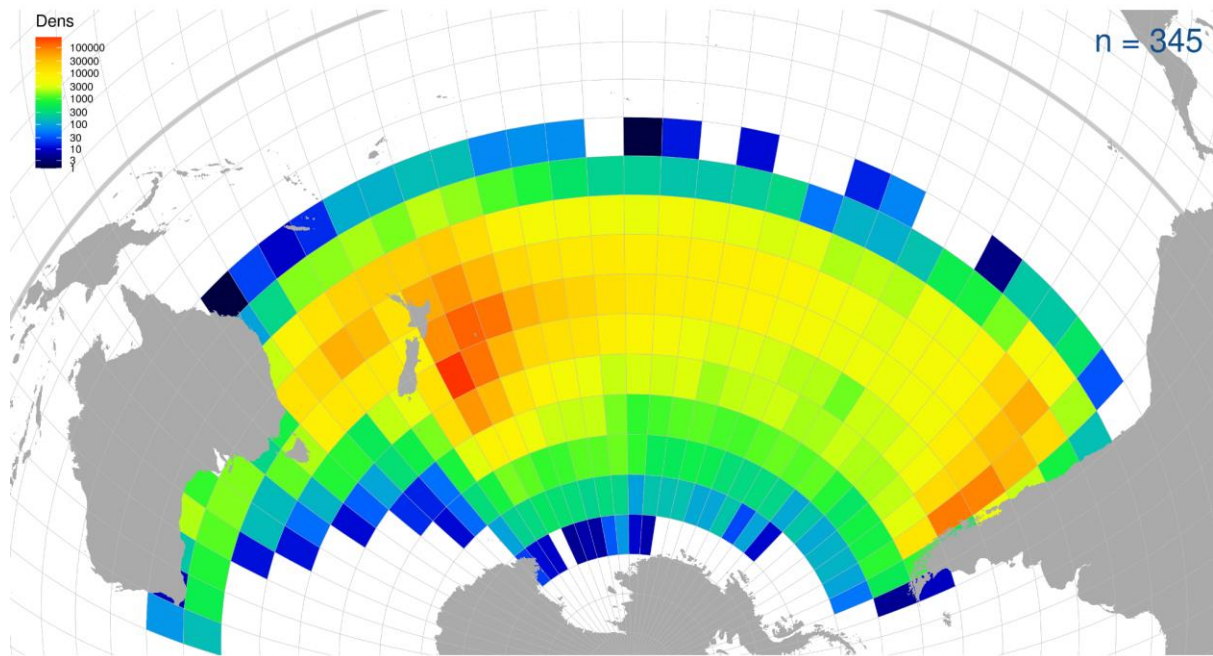


Figure 4. Density (in log-scale) of interpolated tag records for all years and tracked Antipodean albatross individuals combined, at 5-degree resolution. The number of tracks is shown in the top-right corner.

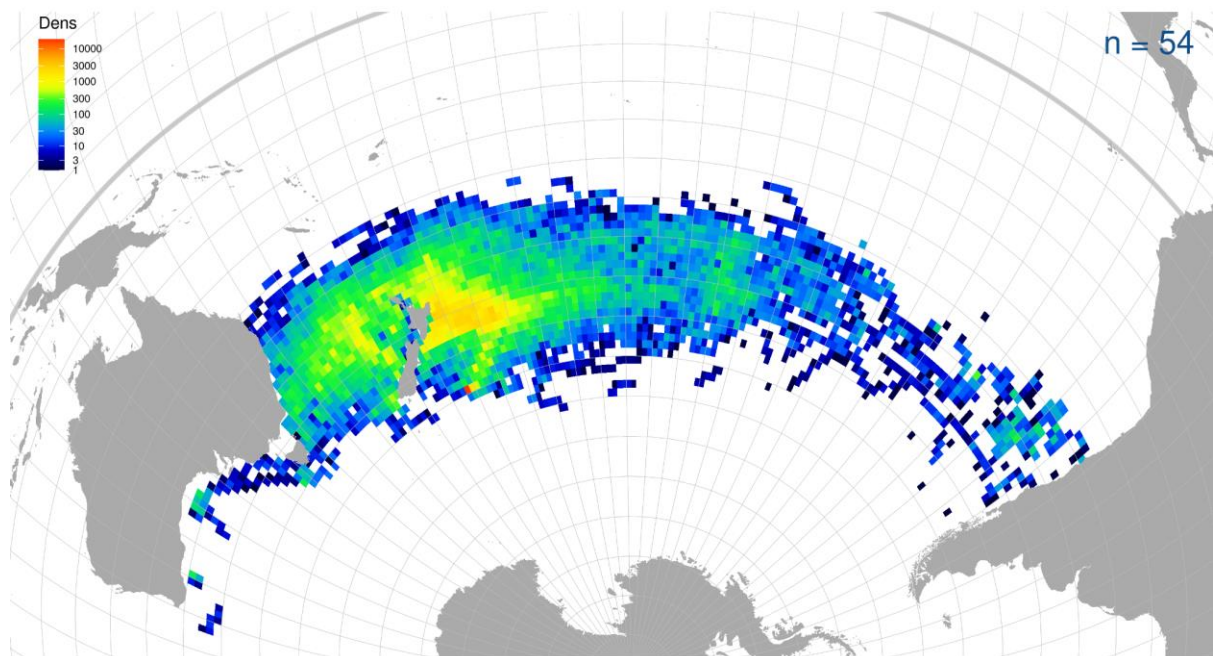


Figure 5. Density (in log-scale) of interpolated tag records for juvenile Antipodean albatross for all years combined, at 1-degree resolution. The number of tracks is shown in the top-right corner.

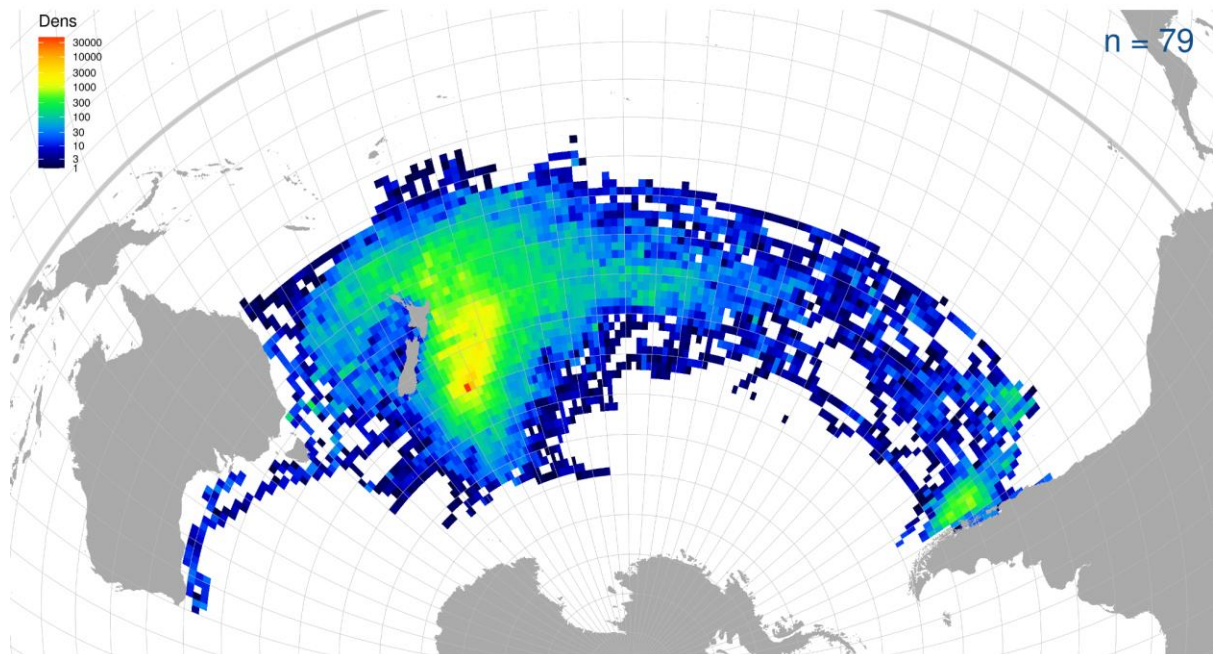


Figure 6. Density (in log-scale) of interpolated tag records for female breeders of Antipodean albatross for all years combined, at 1-degree resolution. The number of tracks is shown in the top-right corner.

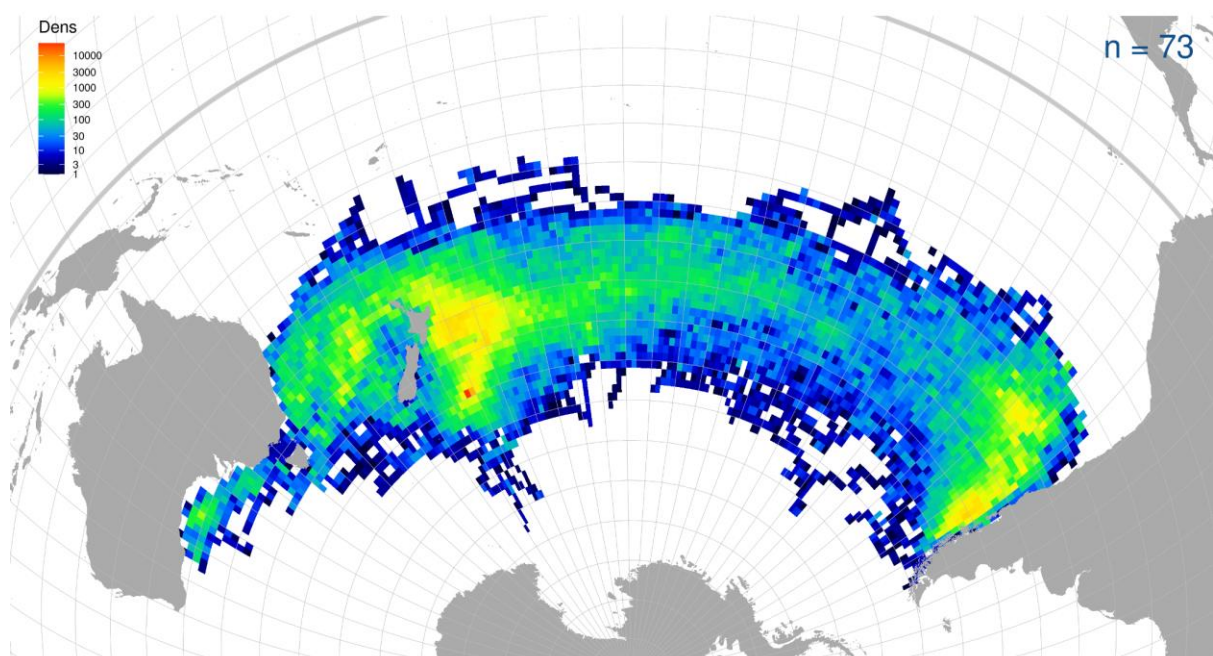


Figure 7. Density (in log-scale) of interpolated tag records for female non-breeders of Antipodean albatross for all years combined, at 1-degree resolution. The number of tracks is shown in the top-right corner.

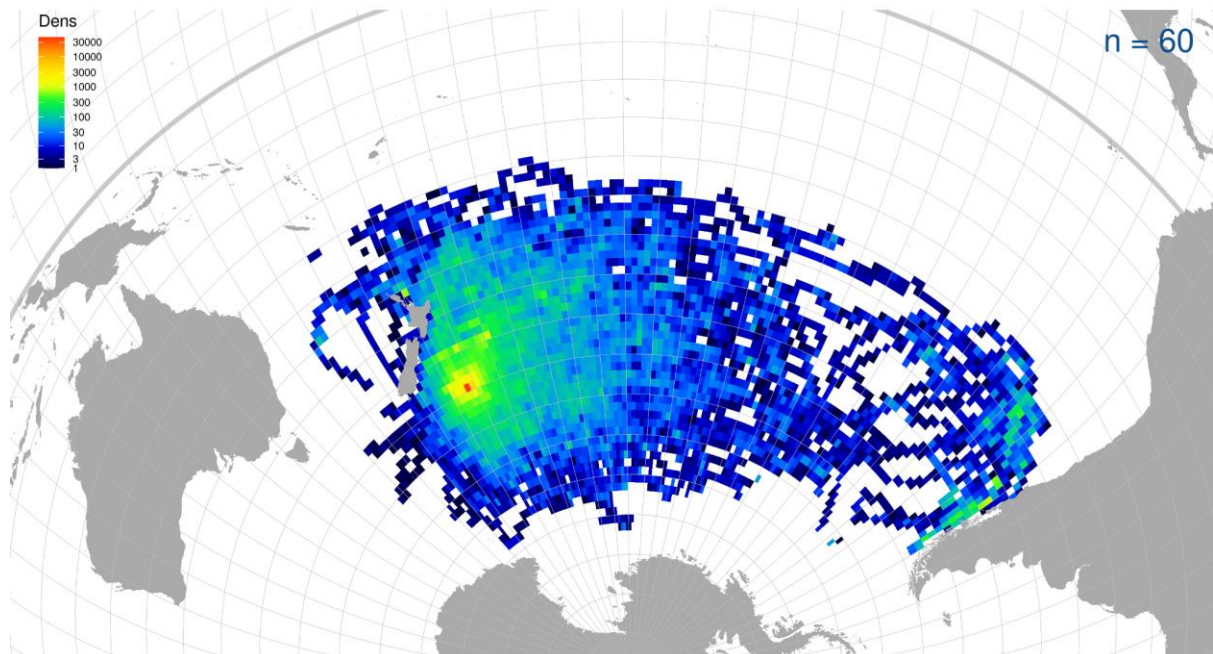


Figure 8. Density (in log-scale) of interpolated tag records for male breeders of Antipodean albatross for all years combined, at 1-degree resolution. The number of tracks is shown in the top-right corner.

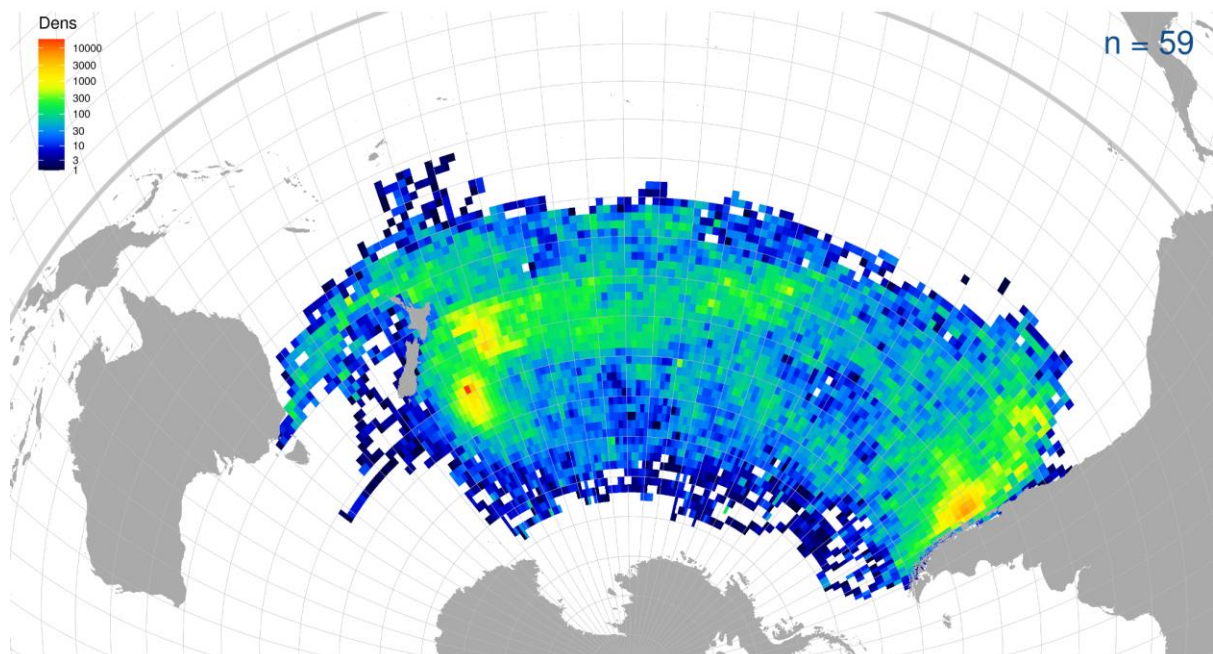


Figure 9. Density (in log-scale) of interpolated tag records for male non-breeders of Antipodean albatross for all years combined, at 1-degree resolution. The number of tracks is shown in the top-right corner.

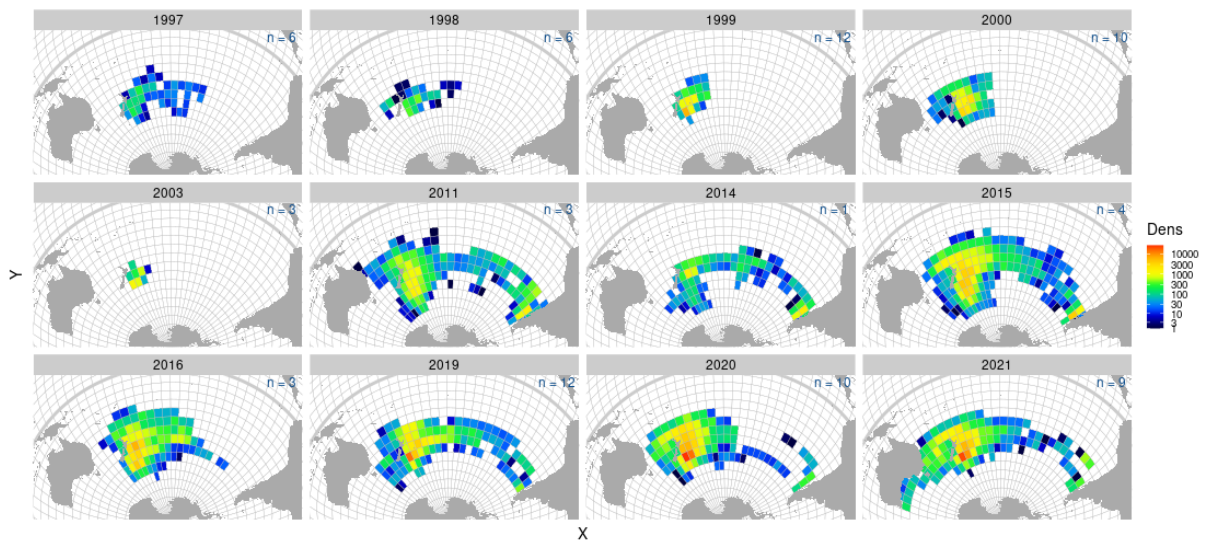


Figure 10. Density (in log-scale) of interpolated tag records for female breeders of Antipodean albatross by observation year, at 5-degree resolution. The number of tracks by year is shown in the top-right corner of each panel.

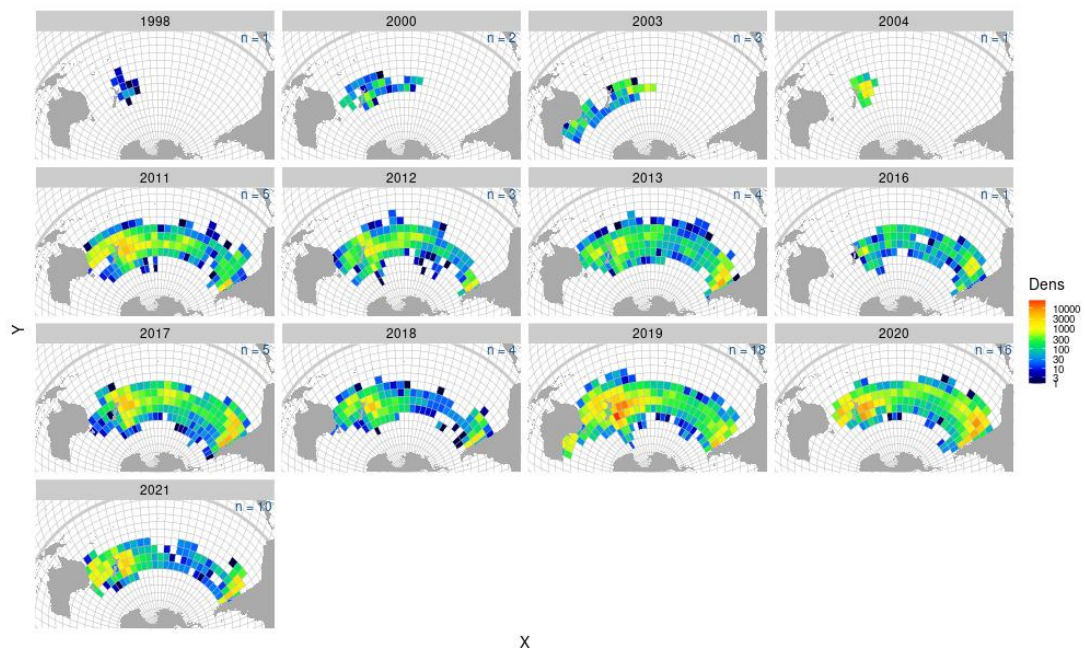


Figure 11. Density (in log-scale) of interpolated tag records for female non-breeders of Antipodean albatross by observation year, at 5-degree resolution. The number of tracks by year is shown in the top-right corner of each panel.

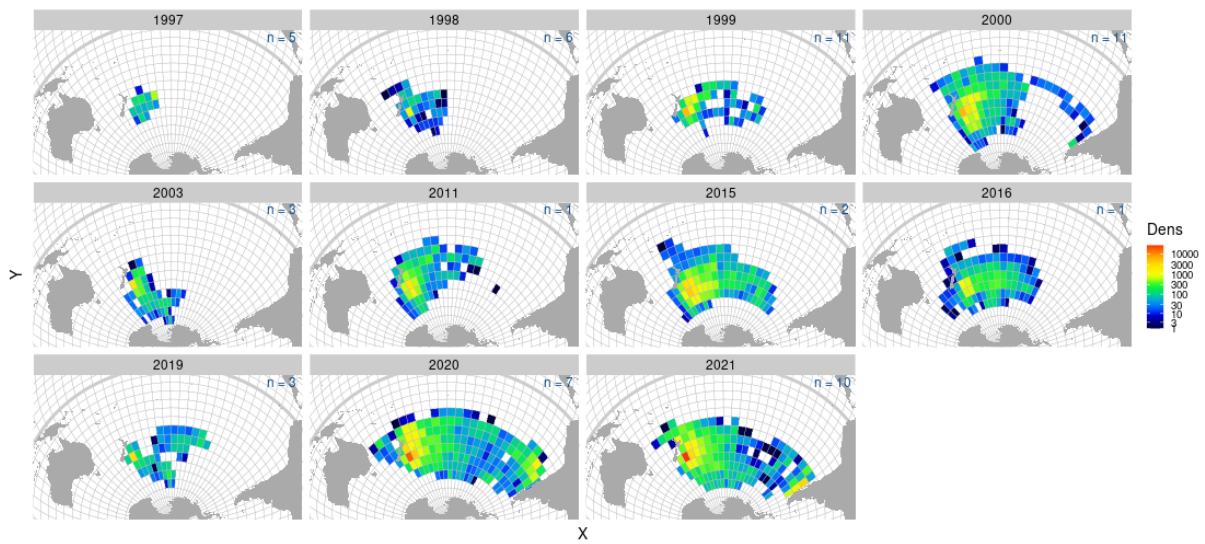


Figure 12. Density (in log-scale) of interpolated tag records for male breeders of Antipodean albatross by observation year, at 5-degree resolution. The number of tracks by year is shown in the top-right corner of each panel.

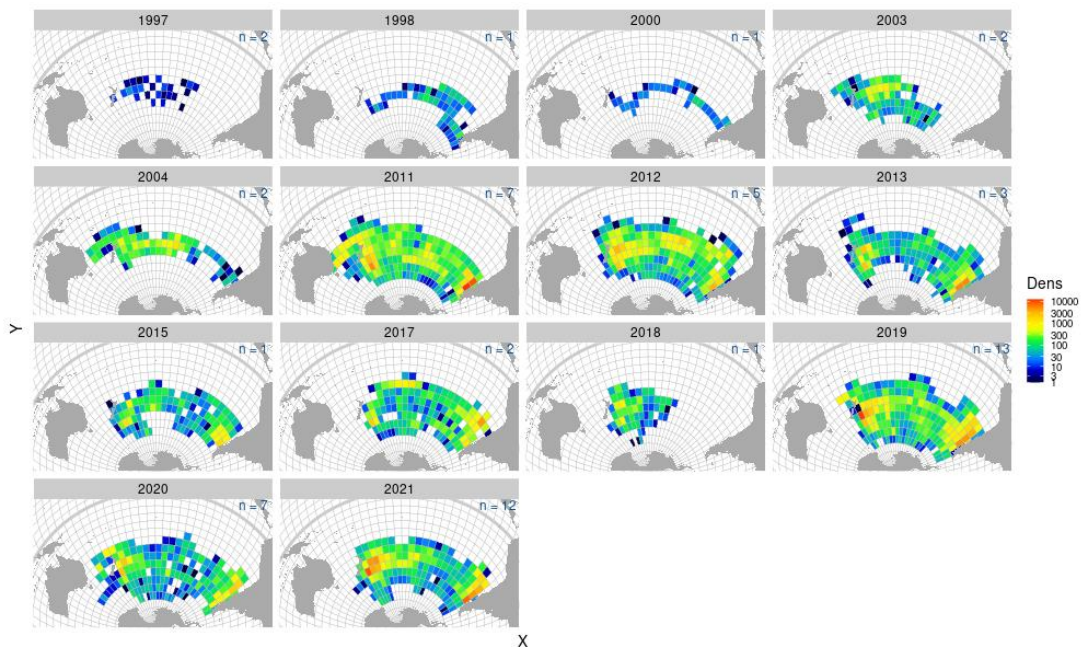


Figure 13. Density (in log-scale) of interpolated tag records for male non-breeders of Antipodean albatross by observation year, at 5-degree resolution. The number of tracks by year is shown in the top-right corner of each panel.

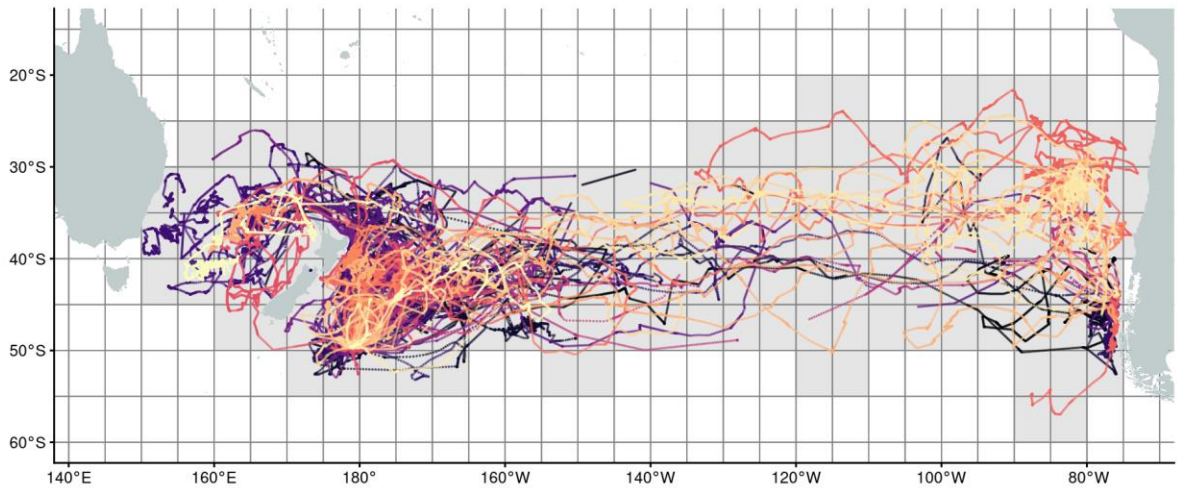


Figure 14. Individual tracks from GPS (global position system) tagging data ($n = 25$) for female non-breeders of Antipodean albatross used for the resampling approach. Each track is shown in a different colour. The 5-degree grid used to estimate the distribution is outlined, with the cells included based on the track information filled in grey.

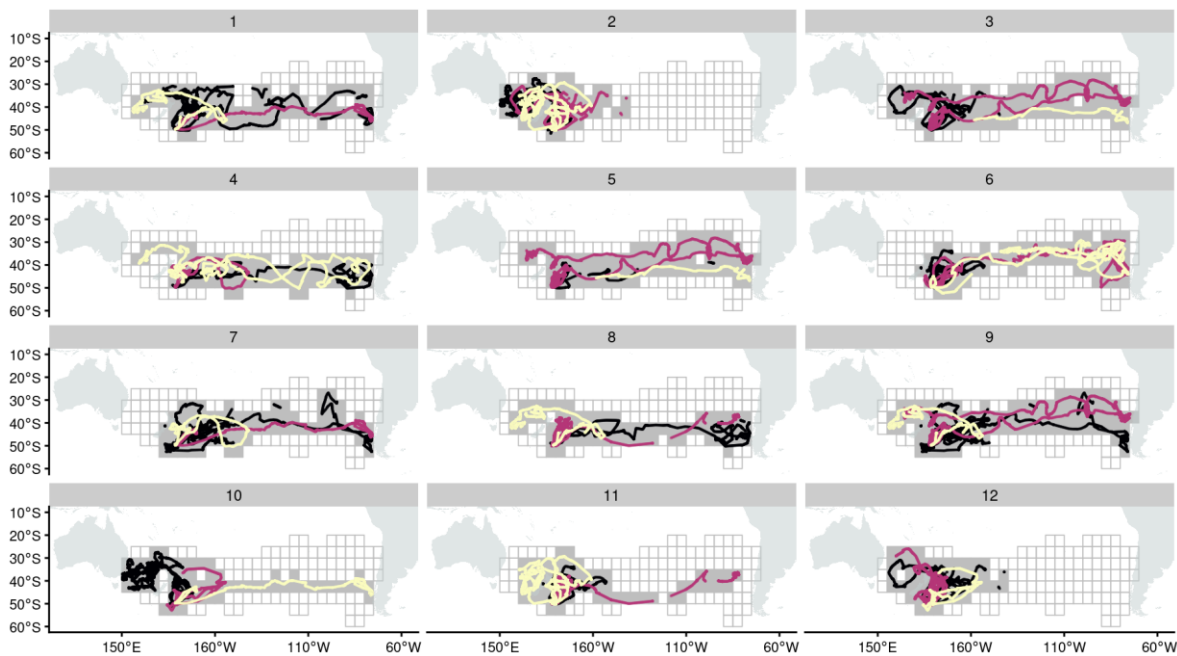


Figure 15. An example of 12 random draws of three tracks from the full set of 25 GPS (global position system) tracks of female non-breeders of Antipodean albatross. The grid cells show the distribution from the full set of tracks, and are filled in grey when they are included as part of the distribution for the current draw of three tracks.

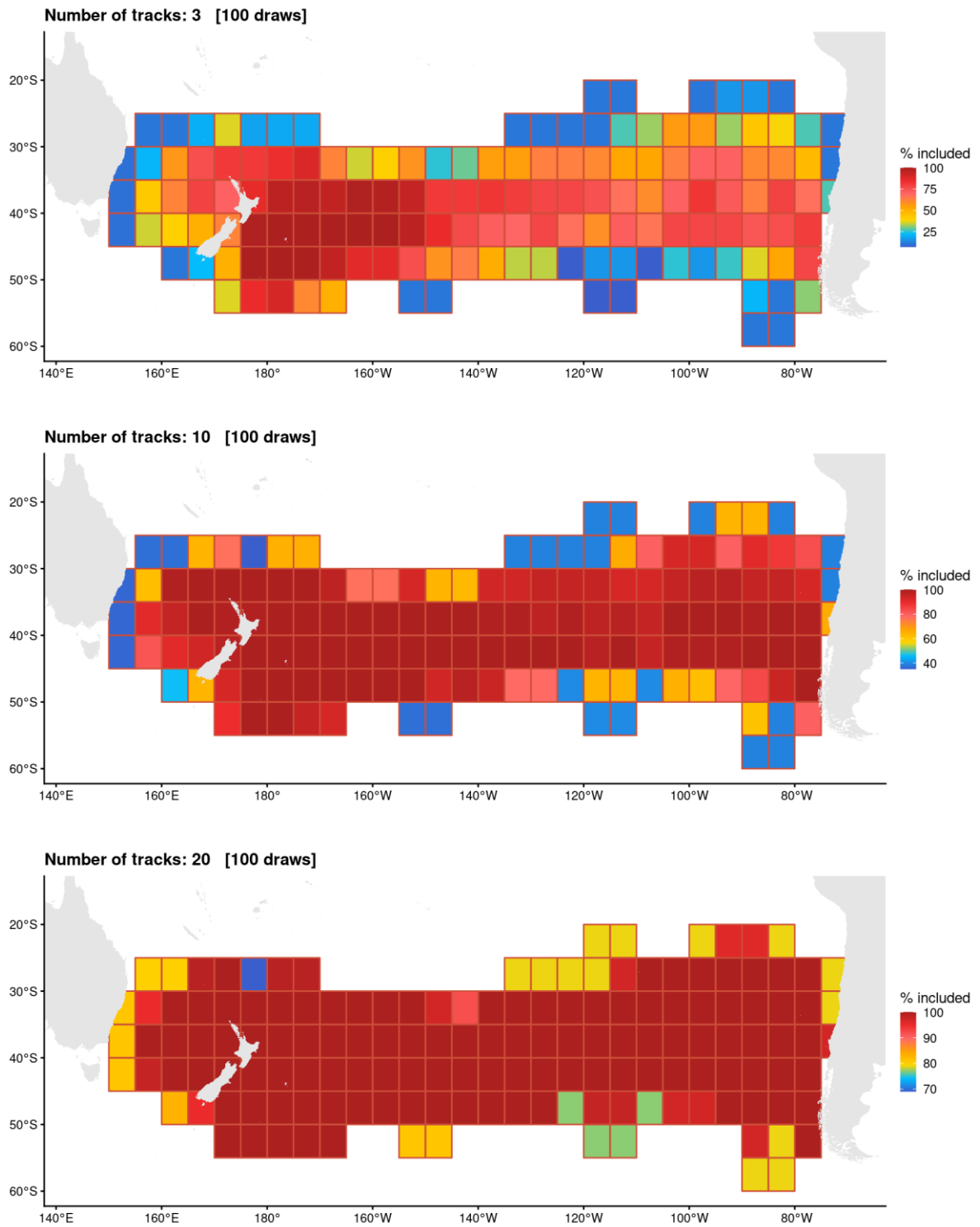


Figure 16. Probability of cell inclusion in the estimated distribution of Antipodean albatross based on the number of tracks used to generate the distribution.

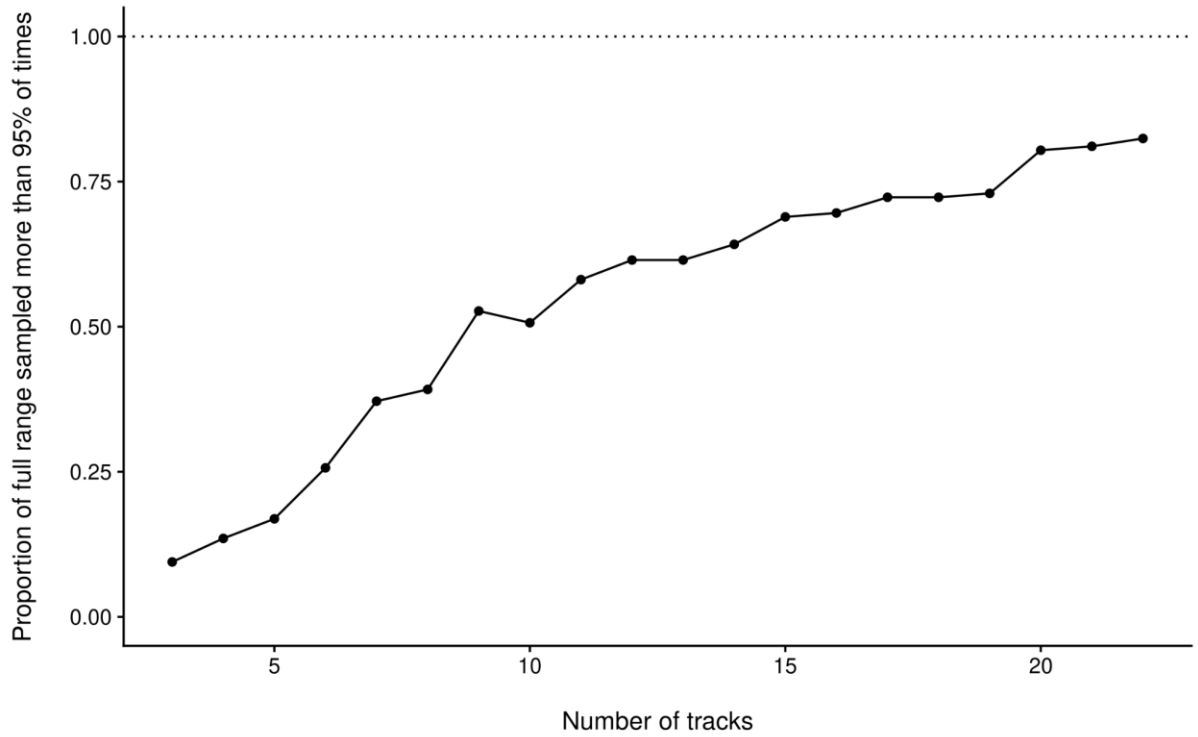


Figure 17. Proportion of the full distribution (estimated based on all 25 GPS tracks of female non-breeders of Antipodean albatross) estimated based on the number of tracks included in the sample. Map cells were considered part of the distribution when they were included in at least 95% of the resampling iterations.

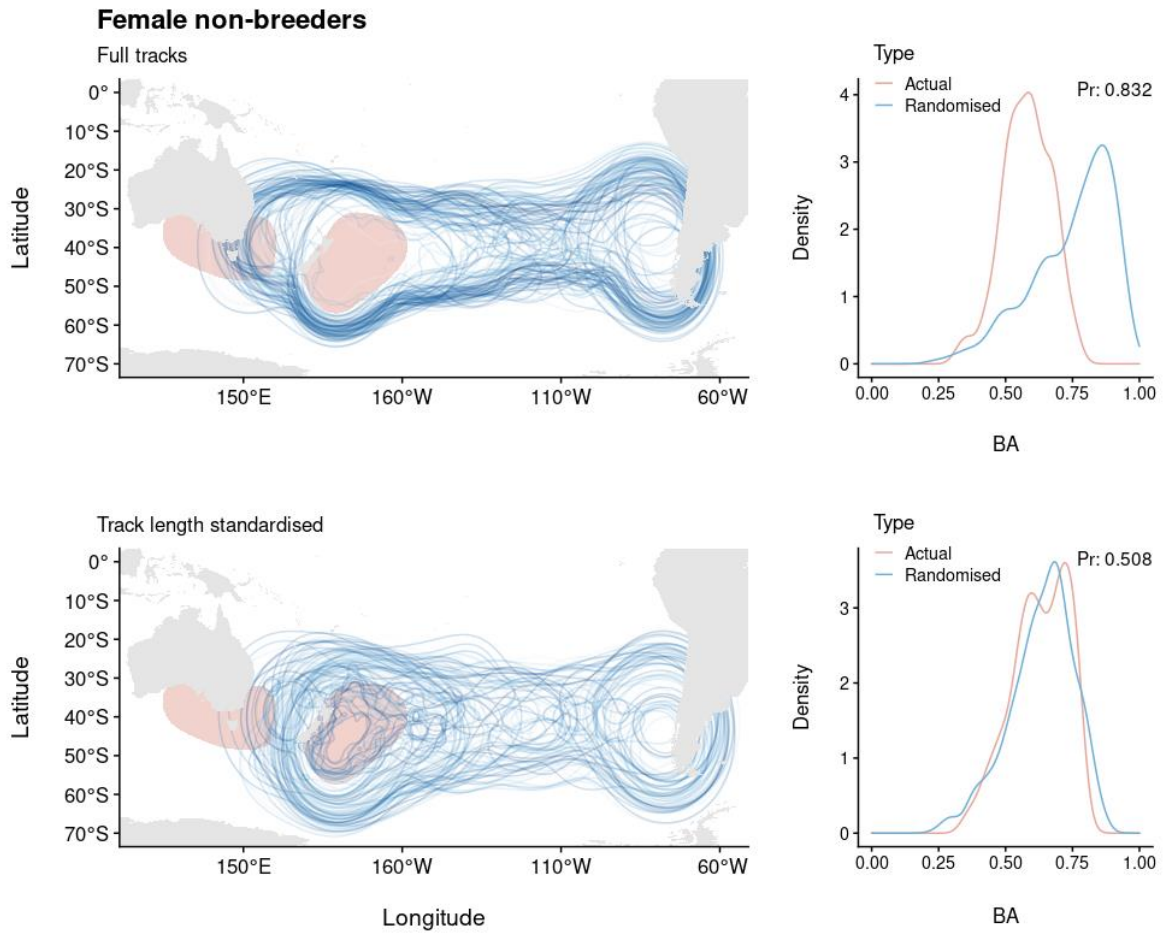


Figure 18. Summary of analyses testing differences in distribution for non-breeder females of Antipodean albatross between the periods 1997–2004 (pre-2004) and 2011–2021 (post-2011). Each map panel compares the 95% kernel density for the pre-2004 period (in red) to a sample of 100 kernel densities generated by resampling tracks from the post-2011 dataset (in shades of blue). Right column compares the distribution of Bhattacharyya’s affinity (BA) metric of overlap for kernels based on the actual period when the track was recorded versus periods randomly assigned to tracks. Top panel shows the results using full tracks from the post-2011 period, and bottom panel shows the results using post-2011 track length standardised to match pre-2004 track lengths.

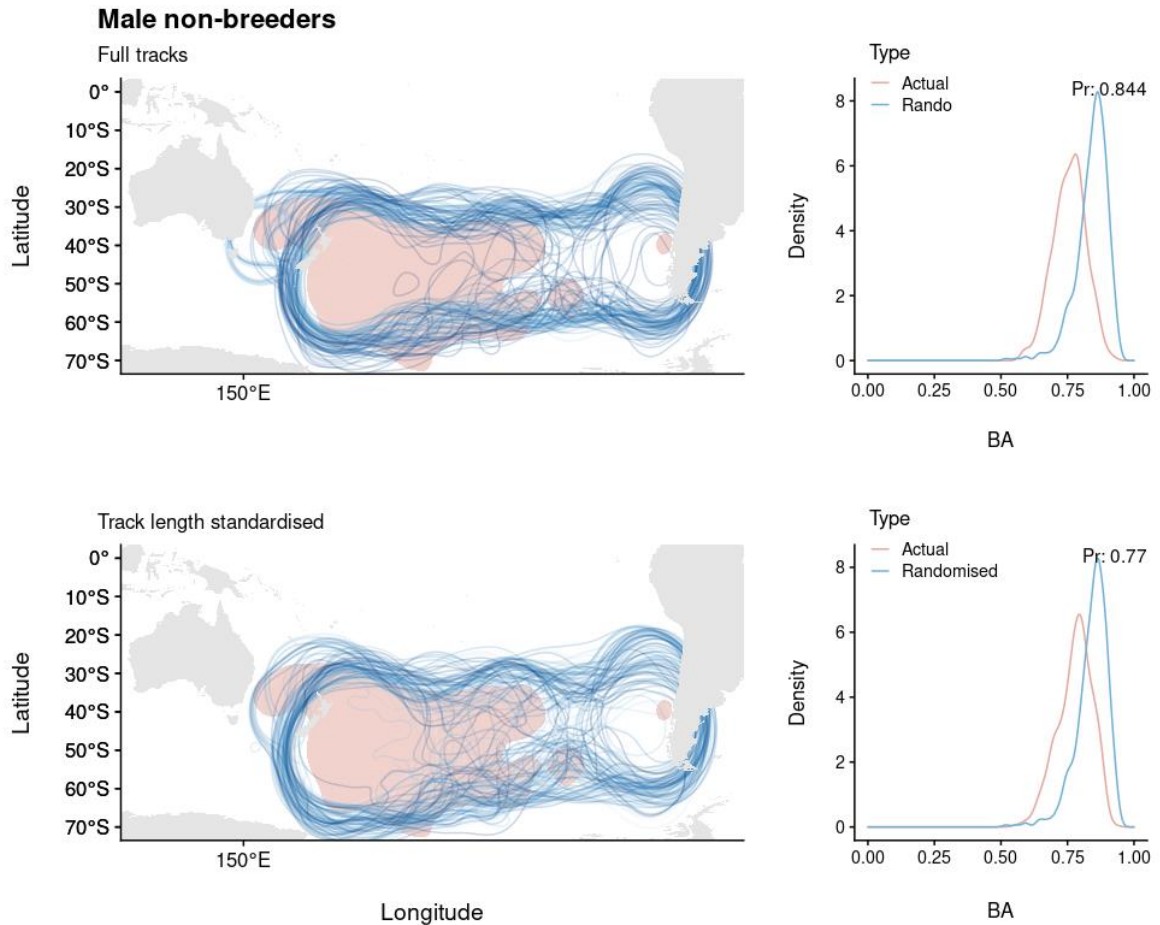
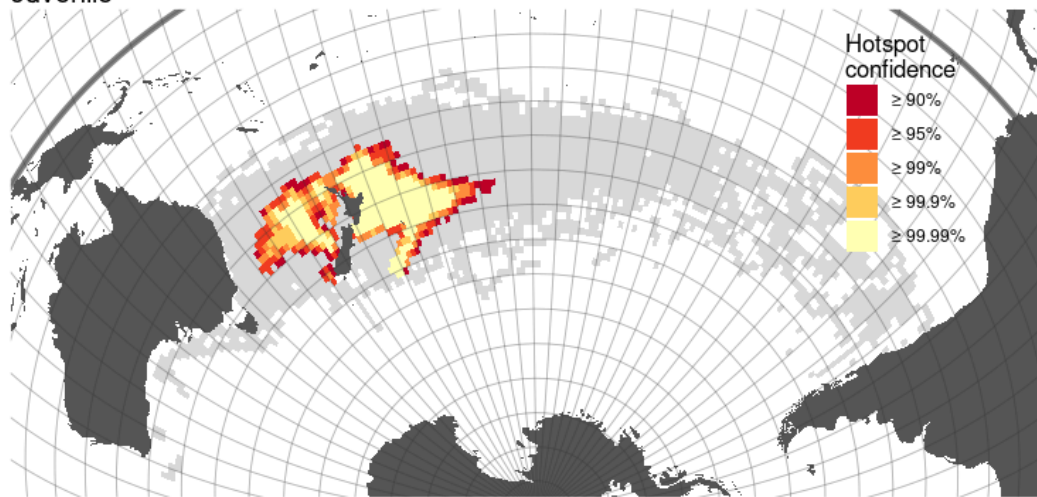
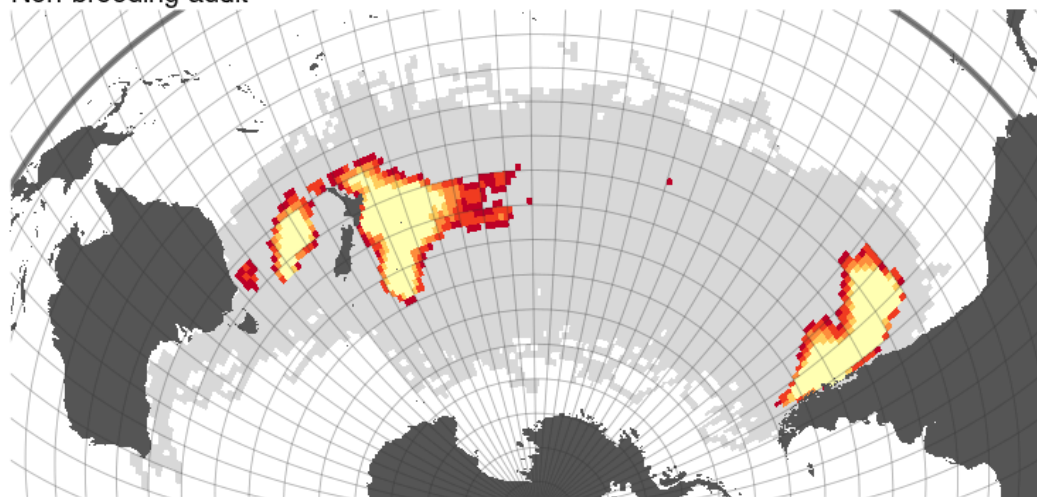


Figure 19. Summary of analyses testing differences in distribution for non-breeder males of Antipodean albatross between the periods 1997–2004 (pre-2004) and 2011–2021 (post-2011). Each map panel compares the 95% kernel density for the pre-2004 period (in red) to a sample of 100 kernel densities generated by resampling tracks from the post-2011 dataset (in shades of blue). Right-most column compares the distribution of Bhattacharyya’s affinity (BA) metric of overlap for kernels based on the actual period when the track was recorded versus periods randomly assigned to tracks. Top panel shows the results using full tracks from the post-2011 period, and bottom panel shows the results using post-2011 track length standardised to match pre-2004 track lengths.

Juvenile



Non-breeding adult



Breeder

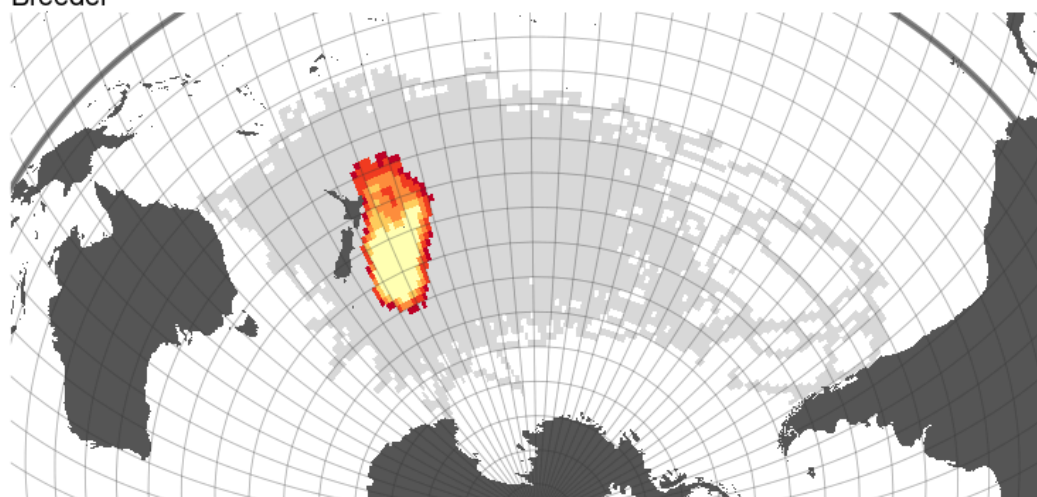


Figure 20. Distribution of high-density hotspots for key Antipodean albatross life stages. Grey shading shows cells with at least one record, cells consisting of a hotspot are shown in yellow to red as a function of the confidence level.

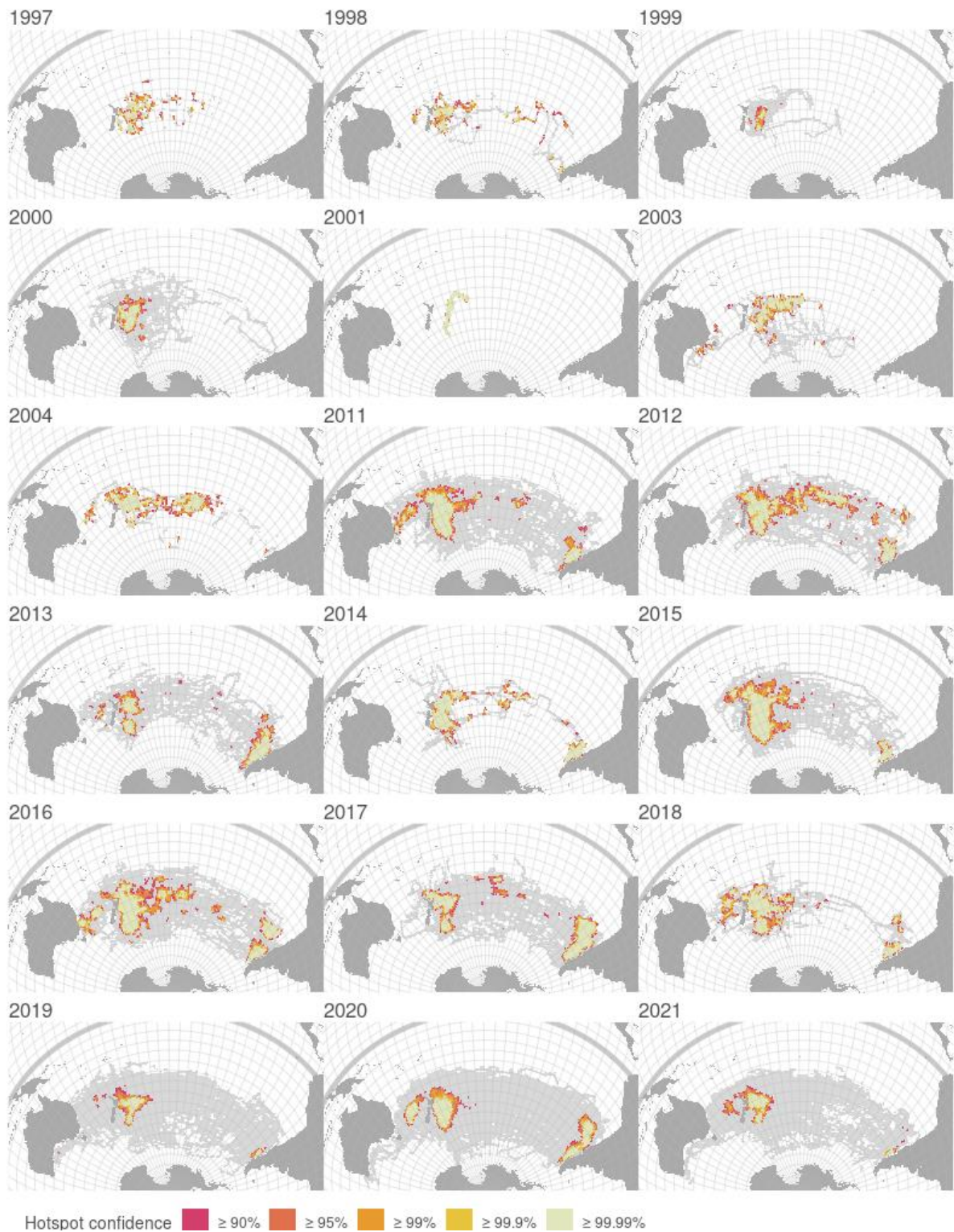


Figure 21. Distribution of high-density hotspots of Antipodean albatross for all years with tagging data, aggregated for all life stages. Grey shading shows cells with at least one record, cells consisting of a hotspot are shown in yellow to red as a function of the confidence level.

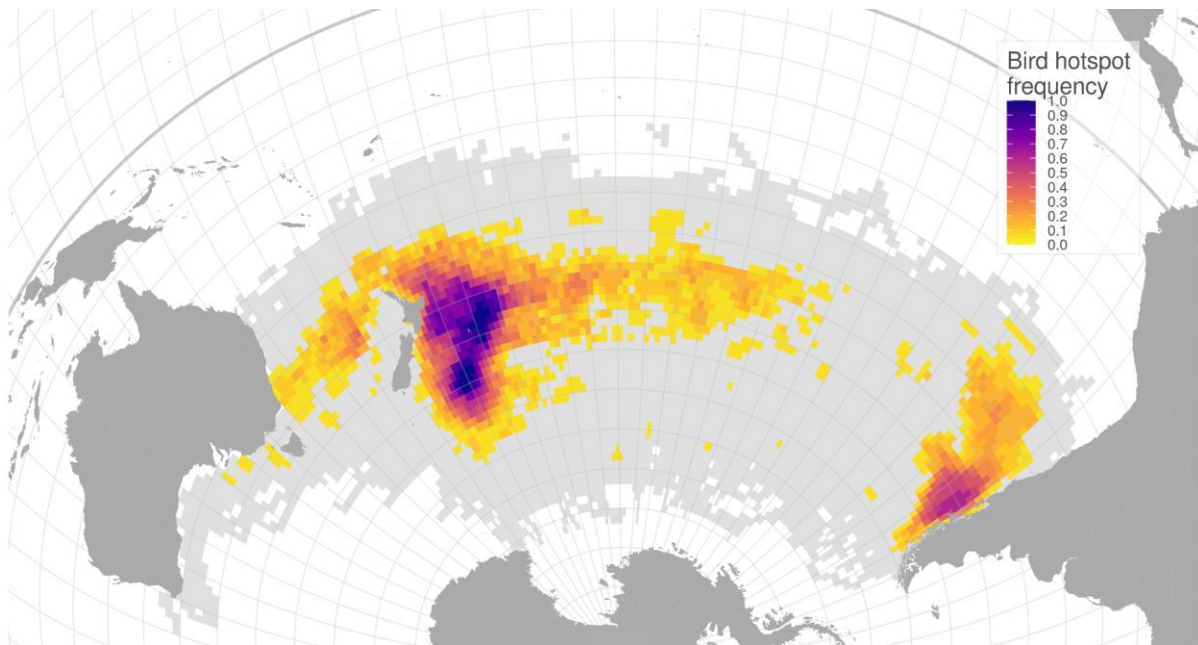


Figure 22. Temporal stability of Antipodean albatross density hotspots. The colour shows the proportion of years when a cell was identified as a hotspot of bird density, at a 99% confidence level. The light grey envelope represents the total extent of the distribution.

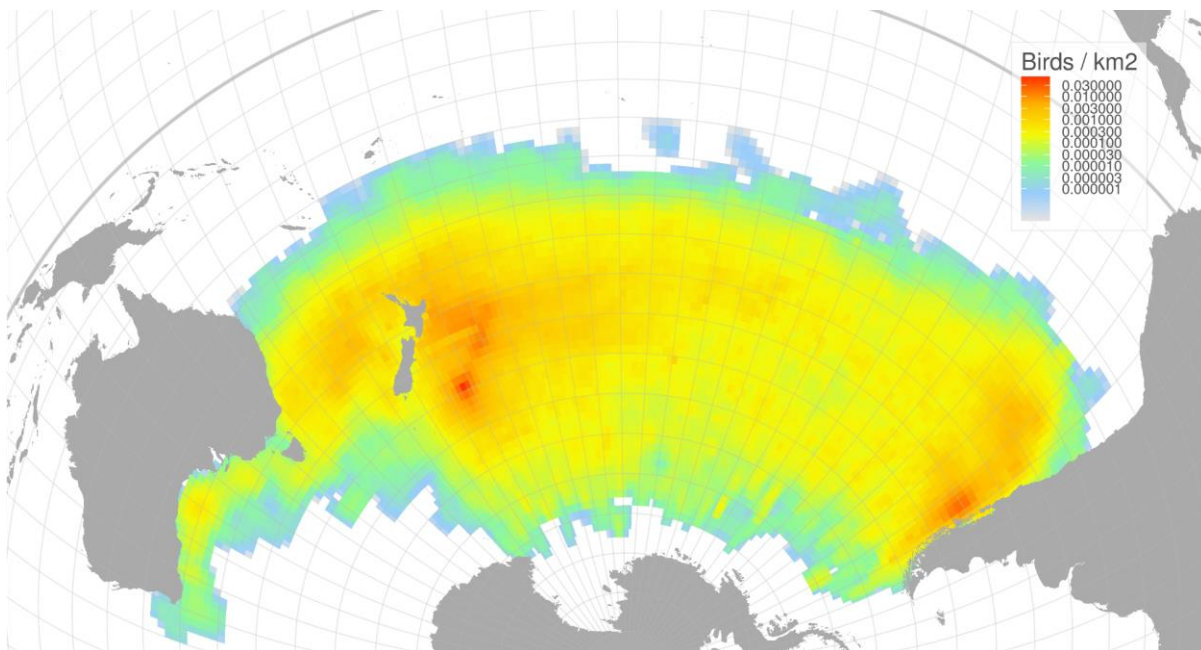


Figure 23. At-sea distribution of Antipodean albatross, after combining the distribution of each demographic stratum across all years between 1997 and 2021, weighted by the number of birds in each stratum obtained from an integrated population model. The colour is shown on a logarithmic scale.

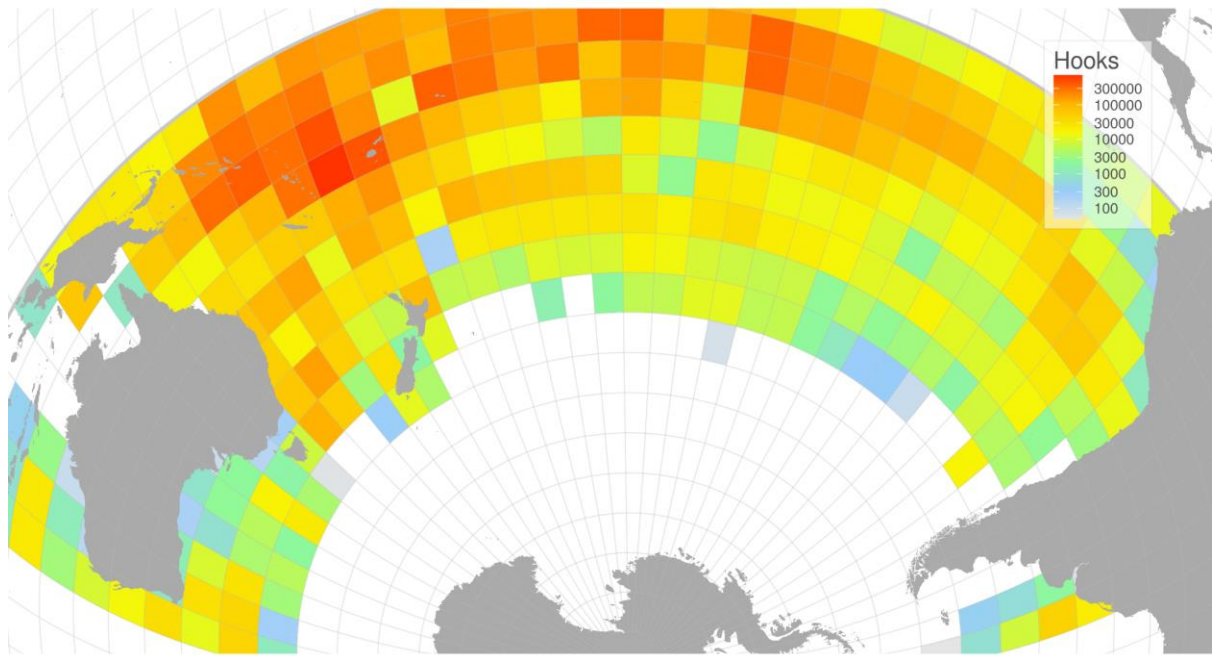
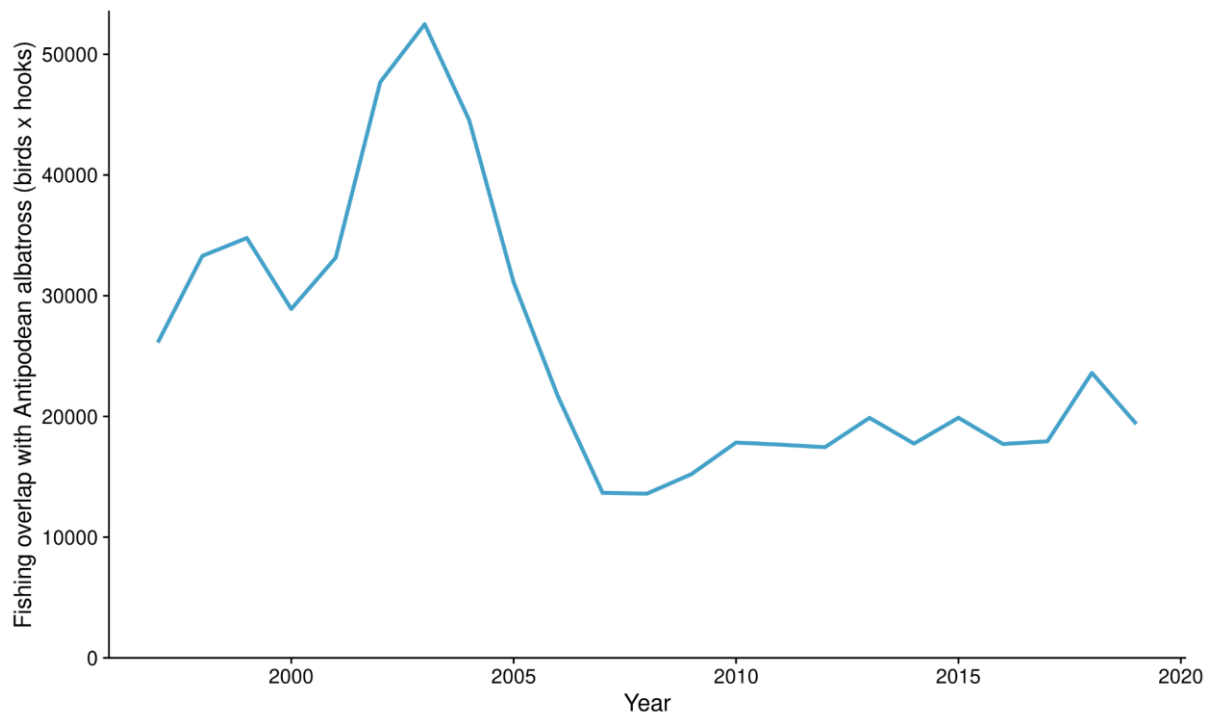


Figure 24. Mean annual surface-longline fishing effort (in hooks) between 1997 and 2019, coloured on a logarithmic scale.

a)



b)

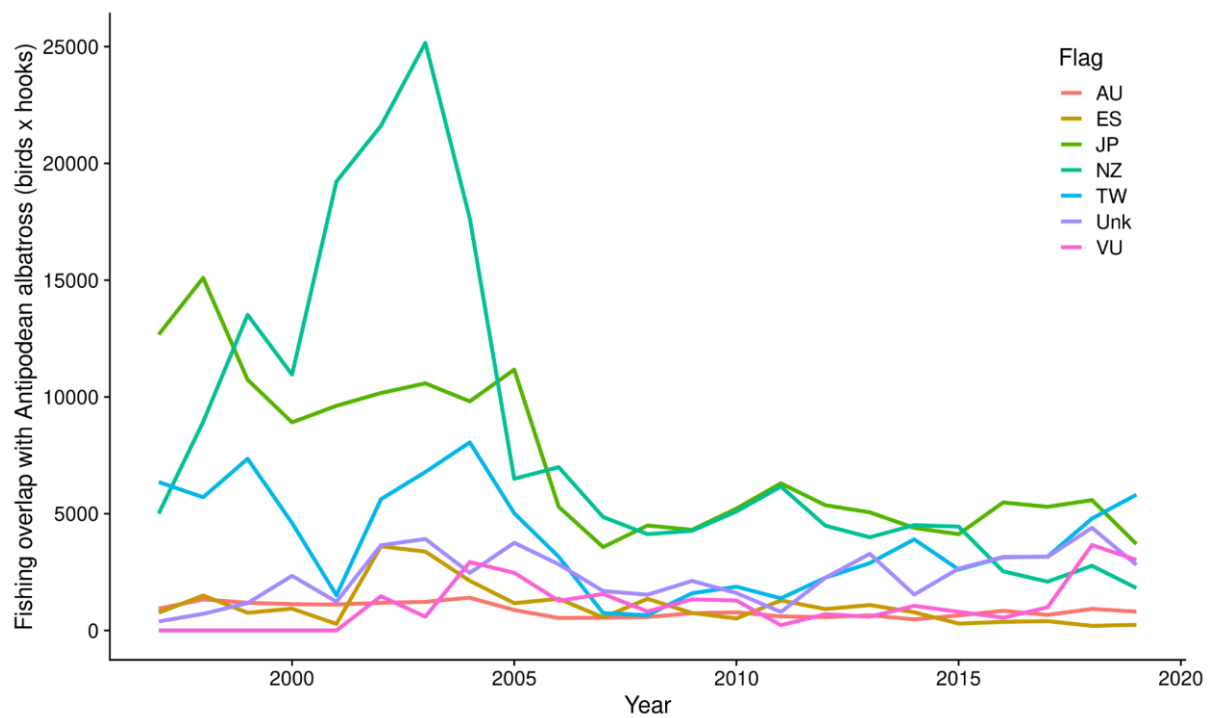


Figure 25. Interannual variability of the overlap between Antipodean albatross and surface-longline fishing effort, a) across all fisheries, and b) by flag for all the flags responsible for 99% of the total overlap.

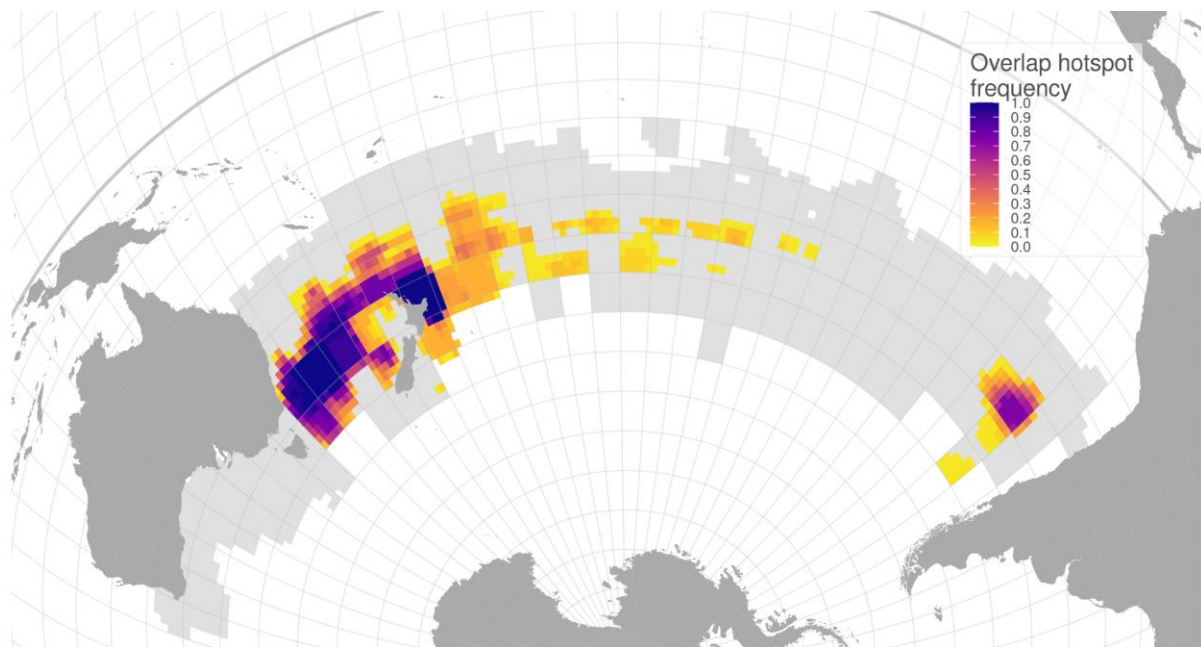


Figure 26. Temporal stability of overlap hotspots between Antipodean albatross and surface-longline fishing effort. The colour shows the proportion of years when each cell was identified as a hotspot of overlap, at a 99% confidence level. The light grey envelope represents the total extent of overlap.

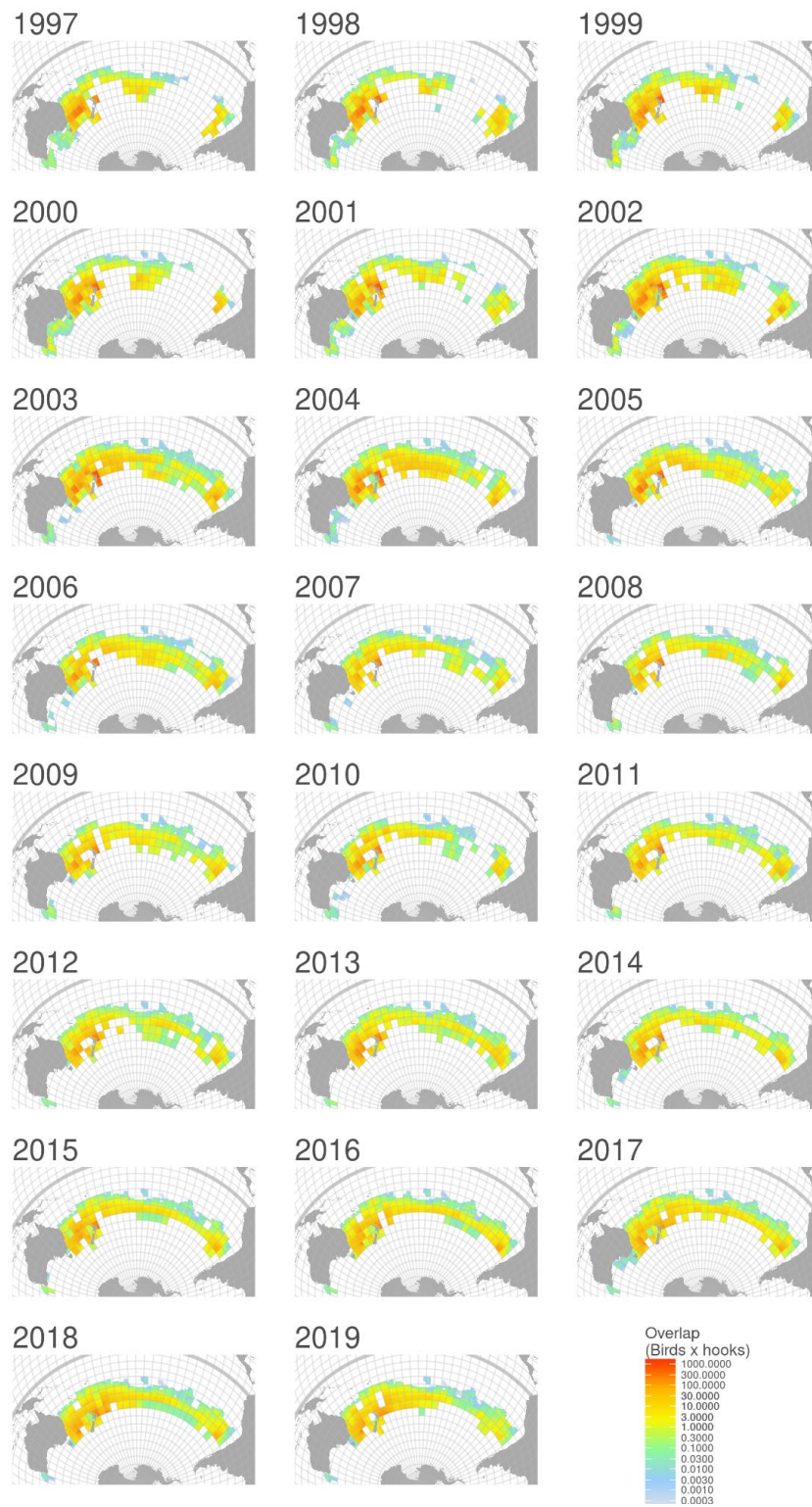


Figure 27. Overlap in the distribution of Antipodean albatross and surface-longline fishing effort in the Southern Hemisphere by year for the period between 1997 and 2019.